Development of a Pellet Extruder with Co-Axial Nozzle for 3D Printing using Inflatable Extrudates

A Thesis

Submitted to the Faculty of Graduate Studies and Research

in Partial Fulfillment of the Requirements

for the Degree of

Master of Applied Science

in

Industrial Systems Engineering

University of Regina

by

Md Ahsanul Habib

Regina, Saskatchewan

August 2024

UNIVERSITY OF REGINA

FACULTY OF GRADUATE STUDIES AND RESEARCH

SUPERVISORY AND EXAMINING COMMITTEE

Md Ahsanul Habib, candidate for the degree of **Master of Applied Science in Industrial Systems Engineering,** has presented a thesis titled, ***Development of a pellet extruder with co-axial nozzle for 3D printing using inflatable extrudates,*** in an oral examination held on **August 8, 2024**. The following committee members have found the thesis acceptable in form and content, and that the candidate demonstrated satisfactory knowledge of the subject material.

External Examiner:	Dr. Md Imran Hasan Tusar, Bowling Green State University
Supervisor(s):	Dr. Mohammad Khondoker, Industrial Systems Engineering
Committee Member:	Dr. SD Jacob Muthu, Energy and Industrial Systems Engineering
Committee Member:	Dr. Wei Peng, Engineering General
Chair of Defense:	Dr. Jinkai Xue, Environmental Systems Engineering

Abstract

Additive manufacturing (AM) has emerged as one of the core components of the fourth industrial revolution, Industry 4.0. Among others, the extrusion AM (EAM) of thermoplastic materials has been named as the most widely adopted technology. Fused filament fabrication (FFF) relies on the commercial availability of expensive filaments; hence pellet extruder-based EAM techniques are desired. Large-format EAM systems would benefit from the ability to print lightweight objects with less materials and lower power consumption which can be possible by using hollow extrudates rather than solid extrudates to print objects. In this work, we designed a custom extruder head and developed an EAM system that allows the extrusion of inflatable hollow extrudates of a relatively wide material choice. By incorporating a co-axial nozzle-needle system, a thermoplastic shell was extruded while the hollow core was generated by using pressurized Nitrogen gas. The ability to print using hollow extrudates with controllable inflation allows printing objects with gradient part density with different degrees of mechanical properties. In this article, the effect of different process parameters namely, extrusion temperature, extrusion speed, and gas pressure were studied using poly-lactic acid (PLA) pellets. Initially, a set of preliminary tests was conducted to identify the maximum and minimum ranges of these parameters that result in consistent hollow extrudates. Later, the parameters were varied to understand how they affect the core diameter and shell thickness of the hollow extrudates. These findings were supported by analyses of microscopic images taken under an optical microscope. In the next phase of our experiment, we printed an inflated cylindrical part using the process parameters derived from the initial set of experiments. We carefully compared the results with the data obtained earlier to ensure accuracy and consistency. Finally, we successfully printed an object with varying densities in different sections.

Keywords: Additive Manufacturing; Extrusion Additive Manufacturing; Hollow Extrudates; Pellet Extrusion; Fused Filament Fabrication.

Acknowledgements

All praise and gratitude are due to Allah, the Lord of the worlds, who bestowed upon me the strength, guidance, and patience to complete this thesis. His infinite mercy and blessings have been my constant source of inspiration throughout this journey. I extend my deepest appreciation and gratitude to my esteemed professor, Dr. Mohammad Khondoker, Assistant Professor in the Industrial System Engineering Department at the University of Regina. Your unwavering support, invaluable guidance, and scholarly wisdom have been instrumental in shaping this thesis and expanding my understanding of the subject matter. Your dedication to excellence and commitment to nurturing your students' intellectual growth have left an indelible mark on my academic and professional development. I am profoundly grateful for your mentorship, encouragement, and constructive feedback, which have challenged me to strive for excellence and to push the boundaries of my knowledge. Your passion for research and your genuine concern for the success of your students have inspired me to pursue academic excellence with diligence and perseverance. I also express my heartfelt appreciation to all the faculty members and staff of the Industrial System Engineering Department for their support and encouragement throughout my academic journey. Your collective efforts have created an enriching and conducive learning environment that has nurtured my intellectual curiosity and scholarly pursuits.

Table of Contents

List of Tables

List of Figures

Transparency Statement

This thesis book incorporates the use of several AI technologies for various purposes throughout its development. The technologies utilized include ChatGPT for concept generation sourcing related parers, Grammarly for grammar checking, Quilbot for paraphrasing, and Scite.ai for finding related papers. The decision to employ these AI tools was made with the intention of enhancing the quality and efficiency of the research process. Each tool serves a specific function aimed at improving different aspects of the thesis book, ranging from idea generation to language refinement and literature review. The utilization of AI technologies in this thesis book does not undermine the intellectual integrity of the work. Rather, it is acknowledged that these tools are employed as aids to augment human capabilities and facilitate the research process. While AI systems contribute to various stages of the project, the ultimate responsibility for the content and conclusions presented herein rests with the author. It is important to note that while AI technologies can offer valuable assistance, they are not infallible and may not always produce optimal results. Therefore, human judgment and oversight were exercised throughout the development of this thesis book to ensure the accuracy, coherence, and integrity of the content. The transparency statement aims to provide clarity regarding the use of AI technologies in the creation of this thesis book, acknowledging their roles and limitations while affirming the authors' commitment to academic integrity and scholarly rigor.

Chapter 1: Introduction

1.1 Background

Additive Manufacturing (AM), often synonymous with 3D printing, has revolutionized the production landscape across various industries by allowing for rapid prototyping, customization, and complex geometry production that is not feasible through traditional manufacturing methods [1,2,3]. Traditionally, additive manufacturing has utilized a range of materials, including polymers, metals, and ceramics, each offering unique properties suitable for specific applications. Among these, thermoplastics have gained prominence due to their versatility, durability, and ease of use [4].

The evolution of additive manufacturing technologies has been marked by continuous innovation aimed at overcoming the limitations of traditional manufacturing methods. The origins of additive manufacturing can be traced back to the 1980s, with the invention of stereolithography (SLA) by Chuck Hull in 1984. SLA worked by curing photopolymer resin layer by layer with ultraviolet (UV) lasers to build 3D objects. This pioneering technology laid the groundwork for subsequent developments in AM, introducing the concept of layer-by-layer fabrication, which remains fundamental to all AM technologies [1,5].

Following SLA, other techniques such as Fused Deposition Modeling (FDM) and Selective Laser Sintering (SLS) were developed. FDM, introduced by Scott Crump in the late 1980s, utilized thermoplastic filaments extruded through a heated nozzle, paving the way for the widespread use of thermoplastics in AM [5].

Thermoplastics have become a material of choice in additive manufacturing due to their thermal behavior, which allows them to be melted, shaped, and solidified repeatedly without significant degradation. This property makes them ideal for processes such as fused deposition modeling (FDM), where the material is extruded through a heated nozzle to build objects layer by layer. However, the conventional use of thermoplastics has been limited to solid extrudates, restricting the ability to create objects with varied internal structures directly through the printing process [6].

The concept of using a pellet extruder in additive manufacturing brings several advantages over traditional filament-based 3D printing. Primarily, pellet extruders utilize raw thermoplastic pellets, which are significantly cheaper and more widely available than manufactured filaments. This not only reduces the material cost but also offers the opportunity to use a broader range of materials, enhancing the versatility of the additive manufacturing process [6,7].

Pellet extrusion technology also aligns well with the principles of sustainable manufacturing. By using thermoplastics in pellet form, the process minimizes waste and energy consumption compared to those that require the manufacturing of filament. This method, therefore, holds potential for scaling up to industrial levels of production without the environmental footprint typically associated with mass manufacturing processes [6,7].

1.2 Problem Statement

Despite the rapid advancements in additive manufacturing technologies, the industry continues to face significant challenges in fabricating objects with complex internal geometries and variable densities directly from the printing process. Current methods predominantly focus on solid material extrusion, limiting the ability to create objects that require internal voids or differentiated density distributions without extensive post-processing or assembly. This limitation is particularly pronounced in applications demanding customized mechanical properties, lightweight structures with high strength, or objects with integrated functionality that relies on varying material composition and structure.

The use of thermoplastics in additive manufacturing, while versatile, has not fully explored the potential of inflatable extrudates to overcome these challenges. Traditional extrusion techniques, such as fused deposition modeling (FDM), restrict the production to solid profiles, lacking the capability to introduce controlled inflation within the extrudate to alter its internal structure during the print process. Furthermore, the adaptation of pellet extruders for additive manufacturing proposes an innovative approach to material deposition, offering advantages in material diversity and cost-effectiveness. However, the integration of pellet extrusion with a mechanism for inflating thermoplastic extrudates remains underexplored, presenting a significant gap in the technology's ability to produce objects with tailored internal properties.

Moreover, the absence of a comprehensive framework for understanding the relationship between extrusion parameters, material properties, and the inflation process hinders the development of standardized methods for producing inflatable thermoplastic extrudates. This gap not only limits the practical application of this innovative approach but also constrains the exploration of its potential to revolutionize the design and functionality of printed objects.

Therefore, this research seeks to address the critical challenge of developing a methodology for additive manufacturing of inflatable thermoplastic extrudates using a pellet extruder. The study aims to explore the mechanics of inflation within the extrusion process, identify the material properties conducive to controlled inflation, and establish the parameters necessary for achieving variable densities and internal structures. By bridging this gap, the research endeavors to unlock new possibilities in additive manufacturing, enabling the creation of objects with unprecedented functional complexity and structural diversity.

1.3 Objective of the study

The objective of the experiment is multifaceted, aiming to explore the capabilities, optimize the processes, and generate samples with this innovative approach. Here's a detailed breakdown of the objectives:

The primary objective is to establish a comprehensive methodology that enables the controlled inflation of thermoplastic extrudates during the additive manufacturing process. This involves determining the optimal conditions under which thermoplastics can be extruded and inflated to achieve desired shapes and structures. The methodology will encompass the selection of suitable materials, the design and calibration of the pellet extruder, and the precise control of process parameters such as temperature, pressure, and extrusion speed.

Another objective of this study is to figure out the relationship among the process parameters and by changing the process parameters how we can control the inflation rate. We want to find the best mix of these settings to control the inflation process well. This will help us make unique and complex objects more efficiently. By doing this, we hope to improve 3D printing techniques to create lightweight and strong parts that can be used in many different ways.

The ability to produce objects with varying densities and internal structures is a key advantage of using inflatable thermoplastic extrudates. This objective aims to explore and optimize the parameters that control the degree and uniformity of inflation within the extrudate. By manipulating factors such as the inflation pressure, timing, temperature, and flow rate the experiment seeks to develop a process that can create complex internal geometries and gradient densities within a single object.

1.4 Significance of the Study

Studying hollow additive manufacturing extrusion is significant for several reasons, each contributing to the advancement of manufacturing technologies and the development of innovative applications across various industries. Hollow structures, characterized by internal voids or cavities, offer unique advantages that are crucial in engineering, design, and material science.

One of the primary benefits of hollow structures is significant weight reduction without compromising structural integrity. This is particularly important in industries such as aerospace, automotive, and robotics, where reducing weight directly translates to improved fuel efficiency, performance, and operational costs. Hollow components can provide the necessary strength and durability while being lighter than their solid counterparts.

Hollow extrusion processes can lead to considerable material savings. By creating components with internal cavities, manufacturers use less raw material, which can reduce production costs and make the manufacturing process more sustainable. This is especially beneficial when working with expensive or scarce materials, such as certain metals and high-performance polymers.

Hollow structures can be designed to optimize mechanical properties, such as strength, stiffness, and flexibility. For example, cellular structures or lattice designs can provide high strength-to-weight ratios, impact resistance, and energy absorption capabilities. These properties are crucial for applications requiring robust yet lightweight components.

Hollow components can offer superior thermal and acoustic insulation properties. The internal voids in hollow structures can reduce heat transfer and sound propagation, making them ideal for applications in building construction, automotive interiors, and electronic device housings. Enhanced insulation properties can improve energy efficiency and user comfort.

Additive manufacturing, particularly with hollow extrusion techniques, enables the creation of highly complex and customized geometries that would be difficult or impossible to achieve with traditional manufacturing methods. This capability is vital for producing tailored solutions in medical implants, aerospace components, and consumer products, where unique shapes and intricate internal structures are required.

By reducing material usage and weight, hollow additive manufacturing can contribute to more sustainable production practices. Lower material consumption means less waste and a smaller environmental footprint. Additionally, lighter components can lead to reduced energy consumption during transportation and operation, further supporting environmental sustainability.

Hollow structures can integrate multiple functions within a single component. For instance, cooling channels, wiring conduits, or reinforcement ribs can be incorporated into the design of a hollow part, enhancing its functionality and reducing the need for additional assembly steps. This integration can simplify designs, reduce manufacturing complexity, and improve overall system performance.

Studying hollow additive manufacturing extrusion is crucial due to its multifaceted benefits, including weight reduction, material savings, enhanced mechanical properties, and the ability to produce complex, customized geometries. The significance of this technology spans various industries, offering innovative solutions that improve efficiency, sustainability, and performance. As additive manufacturing continues to evolve, the development and optimization of hollow extrusion techniques will play a vital role in advancing manufacturing capabilities and enabling new applications. By understanding and leveraging the advantages of hollow structures, manufacturers can create more efficient, cost-effective, and sustainable products, driving progress across numerous fields.

Chapter 2: Literature Review

2.1 Introduction

The term Industry 4.0 has become synonymous with the fourth industrial revolution; a paradigm shift that merges cutting-edge digital technologies with traditional manufacturing processes. Proposed by the German government in 2011, Industry 4.0 aims to revolutionize how products are made, improve operational efficiency, and enhance decision-making across the entire value chain. The vision is to achieve smart manufacturing, technological platforms, market responsiveness, and flexible production while maximizing efficiency and minimizing costs [8,9].

This revolution is reshaping industries by integrating cyber-physical systems, the Internet of Things (IoT), big data, and artificial intelligence (AI) to create smart factories. These factories are capable of self-optimizing and self-configuring, leading to increased efficiency, productivity, and flexibility in production processes. Central to this transformation is the field of advanced manufacturing, which encompasses various innovative techniques and technologies aimed at enhancing manufacturing capabilities and addressing the limitations of conventional methods [10-12].

Recent advancements in manufacturing have significantly enhanced production capabilities, enabling more precise, efficient, and flexible operations. However, these advancements are not without limitations. Traditional manufacturing processes, even with recent improvements, still face several challenges that hinder their full potential. Additive manufacturing (AM), or 3D printing, offers promising solutions to many of these limitations, paving the way for more innovative and sustainable manufacturing practices.

One of the most significant limitations of recent advanced manufacturing is the rigidity and inflexibility of production lines. Traditional advanced manufacturing processes excel in high-volume production. These methods require expensive and time-consuming tooling and molds, making them economically viable only for large production runs. This rigidity limits the ability to quickly adapt to changing market demands or to produce customized products in small batches. While AM may not replace high-volume manufacturing entirely, it shines in specific scenarios. For low-volume or customized production, AM offers unparalleled flexibility. By consolidating assemblies into single parts, AM reduces the need for complex assembly processes, potentially lowering costs and waste. [13]

Another critical limitation is the material waste and inefficiency inherent in subtractive manufacturing processes. Traditional machining involves cutting away material from a larger block to create the desired shape, resulting in significant material waste. This not only increases material costs but also has a substantial environmental impact. Additive manufacturing, on the other hand, uses only the material needed to build the part, significantly reducing waste. This layer-by-layer construction method is particularly advantageous for industries that use expensive or scarce materials, such as aerospace and medical device manufacturing, where minimizing waste is crucial [14].

Energy consumption is another area where traditional manufacturing methods fall short. Many conventional processes are energy-intensive, contributing to high operational costs and a large carbon footprint. For example, injection molding requires significant energy to heat and cool the molds, while machining processes consume substantial energy to operate cutting tools and remove excess material. Additive manufacturing can be more energy-efficient, particularly when producing small batches or complex geometries that would otherwise require multiple manufacturing steps. By simplifying the production process and reducing the need for multiple machines and tools, AM can lower overall energy consumption and associated costs [15].

Quality control and consistency are also challenging in traditional manufacturing, especially when producing complex geometries or intricate designs. Achieving high precision and repeatability often requires multiple steps and meticulous monitoring, increasing the risk of defects and inconsistencies. Additive manufacturing allows for greater design freedom and the ability to produce complex shapes with high precision in a single step. This capability not only improves consistency and quality but also enables the production of parts that would be impossible or impractical to create using traditional methods [16].

Furthermore, the limitations in the scalability of traditional manufacturing methods pose a significant barrier to innovation. The high costs associated with setting up and maintaining production lines for new products can stifle creativity and innovation. Additive manufacturing offers a scalable solution that allows for easy adjustments and modifications to the production process. This scalability fosters innovation by enabling rapid iteration and testing of new designs, accelerating the development of new products and technologies [17].

Traditional manufacturing methods require businesses to maintain a stockpile of parts to handle emergency repGass or unexpected spikes in customer demand. This practice can result in significant amounts of capital being tied up in inventory, which could be more effectively utilized in other areas. In contrast, additive manufacturing enables businesses to produce parts on-demand, reducing the financial burden associated with maintaining extensive inventories [14].

Additive manufacturing is transforming product design and production, notably through its application in distributed manufacturing. This decentralized production model utilizes a network of small-scale printers to create goods. This approach offers several benefits compared to traditional manufacturing methods. It enables production closer to the point of demand, thereby lowering transportation costs and reducing lead times. It also provides designers with enhanced flexibility to tailor products for specific users or applications. Additionally, it addresses supply chain issues by ensuring that additive materials are readily available and allowing for the immediate production of required parts [16].

While recent advancements in traditional manufacturing have significantly improved production capabilities, several inherent limitations persist. The rigidity and inflexibility of production lines, material waste, high energy consumption, and challenges in quality control and scalability are significant barriers that can be mitigated by additive manufacturing or 3D printing, which is another cornerstone of Industry 4.0. By offering greater flexibility, efficiency, and design freedom, AM addresses these limitations and opens up new possibilities for innovative and sustainable manufacturing practices. As technology continues to evolve, the integration of additive manufacturing into traditional production processes will likely become more prevalent, driving further advancements and transforming the manufacturing landscape.

2.2 The Evolution of Additive Manufacturing

Additive manufacturing (AM), commonly known as 3D printing, has evolved remarkably since its inception. The concept of additive manufacturing dates back to 1980 when Hideo Kodama of Nagoya Municipal Industrial Research Institute filed the first patent application for a rapid prototyping system using photopolymers. His method involved using UV light to harden materials layer by layer, but it was never commercialized [18]. Since then AM has been diversified into various techniques, each offering unique capabilities and applications. In 1983, Charles Hull developed the first working 3D printing process known as Stereolithography (SLA). Hull's method involved curing layers of photopolymer resin with ultraviolet light, leading to the creation of 3D Systems Corporation and the first 3D printing patent in 1986 [19]. This marked the commercial beginning of additive manufacturing. Digital Light Processing (DLP) technology, a variation of

SLA, was introduced by Texas Instruments in 1987 and later adapted for 3D printing. DLP uses a digital micromirror device to project light and cure photopolymer resin layer by layer. This technology allows for high-resolution prints and faster curing times compared to traditional SLA [20].

Carl Deckard and his team at the University of Texas developed Selective Laser Sintering (SLS) in 1988. This technique uses a laser to sinter powdered material, binding it together to create a solid structure. Deckard filed a patent for SLS, which was later commercialized by DTM, Inc., and eventually acquired by 3D Systems. SLS Enabled the use of powdered materials, providing versatility in materials such as plastics, metals, and ceramics [21]. In the same year, 3D Systems began selling the SLA-1, marking the entry of the first commercial rapid prototyping printer into the market. [22]

In the following year 1989, Scott and Lisa Crump patented Fused Deposition Modeling (FDM), a technique where thermoplastic material is extruded layer by layer to build a part. This method led to the founding of Stratasys, Inc., which became a key player in the 3D printing industry [23].

In the early 1990s, Helisys, Inc. developed Laminated Object Manufacturing (LOM). This process involves laminating layers of adhesive-coated paper, plastic, or metal together, and then cutting them to shape with a laser or blade. LOM is known for producing large, relatively inexpensive parts quickly [24].

Electron Beam Melting (EBM) was developed in the late 1990s by Arcam AB, a company founded in Sweden. EBM uses an electron beam to melt metal powder layer by layer, creating highly dense and strong metal parts. This technology is particularly useful in aerospace and medical implant industries [25].

Binder Jetting, developed at MIT in the 1990s, involves the selective deposition of a binding agent onto a powder bed, layer by layer. This process allows for the production of parts in various materials, including metals, ceramics, and sands, often used for molds and cores in metal casting [26].

Material Jetting, which emerged in the early 2000s, is akin to inkjet printing. Droplets of photopolymer or wax are selectively deposited and cured with UV light. This technique is known for its ability to produce parts with multiple materials and colors, offering fine details and smooth surfaces [27].

Today, additive manufacturing is recognized for its ability to create complex geometries that would be impossible or prohibitively expensive to produce using traditional manufacturing methods. This capability is particularly beneficial in the aerospace sector, where weight reduction is crucial. Companies like Boeing and Gasbus utilize AM to produce lightweight components that reduce fuel consumption and improve Gascraft performance. According to Wohlers Associates, the aerospace industry has been one of the earliest adopters of AM, with significant investments in research and development to integrate these technologies into mainstream production [28].

The healthcare industry has also embraced additive manufacturing, leveraging its potential to create patient-specific medical devices and prosthetics. Customization is a significant advantage of AM, allowing for the production of implants tailored to individual patients' anatomies, thereby improving fitness and functionality. Bioprinting, a specialized branch of AM, is pushing the boundaries by enabling the fabrication of tissue structures using living cells. Research by Murphy and Atala (2014) highlights the advancements in bioprinting, suggesting a future where it could be possible to print organs for transplantation, thereby addressing the critical shortage of donor organs [29].

In the automotive industry, additive manufacturing is revolutionizing the way vehicles are designed and produced. Companies such as General Motors and Ford are using AM for prototyping and producing parts with complex structures that enhance performance and reduce weight. The ability to rapidly prototype new designs accelerates the development process, enabling manufacturers to bring innovative products to market faster. A study underscores the impact of AM on the automotive sector, emphasizing its role in enabling more efficient and flexible manufacturing processes [30].

Despite these advancements, additive manufacturing is not without its challenges. One significant limitation is the speed of production. While AM is ideal for prototyping and small-batch production, it is often slower than traditional methods for mass production. Efforts are underway to address this limitation, with companies developing faster printing technologies and more efficient materials. For instance, Continuous Liquid Interface Production (CLIP) by Carbon 3D promises to speed up the printing process significantly, making AM more viable for large-scale production [31].

Another challenge is the cost of materials. Although the cost of 3D printers has decreased, the materials used in AM, especially high-performance polymers and metals, remain relatively expensive. However, ongoing research aims to develop more affordable and versatile materials without compromising quality. The development of new materials, such as biodegradable polymers and advanced composites, is expected to expand the applications of AM and reduce costs.

Quality control and standardization are additional hurdles that the industry must overcome. Ensuring consistent quality in AM parts can be challenging due to variations in the printing process and material properties. The development of rigorous standards and certification processes is essential to guarantee the reliability and safety of AM-produced parts. Organizations like ASTM International and ISO are working on establishing such standards to promote widespread adoption and trust in AM technologies [32].

Sustainability is another area where additive manufacturing is making strides. Traditional manufacturing processes often generate significant waste, but AM's layer-by-layer approach can minimize material waste. Furthermore, the ability to produce parts on-demand reduces the need for large inventories, thereby lowering storage costs and waste from unsold products. The potential of AM to contribute to more sustainable manufacturing practices, emphasizing its role in reducing material consumption and enabling the use of recycled materials is recognized everywhere [13].

The current scenario of additive manufacturing is marked by rapid advancements, broadening applications, and ongoing efforts to overcome its challenges. Industries such as aerospace, healthcare, and automotive are at the forefront of adopting AM technologies, leveraging their benefits to enhance performance, customization, and efficiency. Despite facing challenges related to production speed, material costs, quality control, and standardization, the continuous innovation in AM processes and materials holds promise for even more significant industrial transformation. As research and development in this field continue to progress, additive manufacturing is poised to become an even more integral part of modern manufacturing, driving forward the capabilities and sustainability of industrial production.

2.3 Fused Deposition Modeling: The most popular AM method

Fused Deposition Modeling (FDM) has emerged as the most popular method among the various AM methods. FDM, also known as Fused Filament Fabrication (FFF), involves the layer-by-layer deposition of thermoplastic materials to create three-dimensional objects from digital models. The widespread adoption of FDM can be attributed to several factors, including its affordability, ease of use, and versatility.

One of the primary reasons for the popularity of FDM is its cost-effectiveness. FDM printers are generally less expensive than other types of 3D printers, making the technology accessible to a wide range of users, from hobbyists and educators to professional engineers and designers. The relatively low cost of FDM printers has democratized access to 3D printing technology, fostering innovation and experimentation across various fields. Additionally, the cost of materials for FDM is relatively low. Thermoplastic filaments such as PLA (polylactic acid) and ABS (acrylonitrile butadiene styrene) are widely available and affordable, further reducing the overall cost of using FDM technology [33].

Ease of use is another significant factor contributing to the popularity of FDM. The technology is straightforward and user-friendly, requiring minimal setup and maintenance. Users can quickly learn to operate FDM printers, making them suitable for educational purposes and entry-level applications. The simplicity of FDM technology allows for rapid prototyping, enabling designers and engineers to iterate and refine their designs quickly. This capability is crucial in industries such as product development and engineering, where time-to-market is critical [34].

FDM is also valued for its versatility. It supports a wide range of thermoplastic materials, each with distinct properties that can be tailored to specific applications. For instance, PLA is biodegradable and suitable for environmentally friendly applications, while ABS offers high strength and durability for functional prototypes and end-use parts. Advances in filament technology have further expanded the range of materials available for FDM, including composites, flexible filaments, and high-performance engineering plastics. This versatility allows FDM to be used in various industries, including automotive, aerospace, healthcare, and consumer products [35].

One of the significant areas of advancement in FDM technology is the development of composite filaments. Researchers have been incorporating various fillers such as carbon fibers, glass fibers, and metal powders into thermoplastic matrices to create composite materials with superior mechanical properties. These composites offer enhanced strength, stiffness, and thermal resistance, making FDM-printed parts more suitable for demanding applications in aerospace, automotive, and other high-performance industries [14].

Another exciting development in FDM research is the improvement of multi-material printing capabilities. Multi-material FDM allows for the fabrication of parts with varying properties within a single print, enabling the creation of more complex and functional components. This capability is particularly beneficial for producing parts that require different material characteristics, such as flexible joints combined with rigid structures. Studies have shown that multi-material FDM can significantly enhance the functionality and versatility of printed objects, opening new possibilities for custom manufacturing and prototyping [36].

Despite its advantages, FDM has several limitations. One significant limitation is the relatively low resolution and surface finish of FDM-printed parts compared to other AM methods such as Stereolithography (SLA) or Selective Laser Sintering (SLS). The layer-by-layer deposition process of FDM can result in visible layer lines and rough surfaces, which may require post-processing to achieve a smooth finish. Additionally, the mechanical properties of FDM parts can be anisotropic, meaning they are dependent on the orientation of the print layers. This anisotropy can limit the structural integrity and performance of parts in certain applications [37].

Another limitation of FDM is the size of the build envelope. While large-format FDM printers are available, they are often more expensive and less accessible than standard-sized machines. This limitation can restrict the size of parts that can be printed, necessitating the assembly of multiple smaller components for larger projects. Furthermore, the speed of FDM printing can be slower than other AM methods, particularly for high-resolution or complex geometries, which can impact production efficiency and throughput [28].

2.4 Pellet Extrusion-Based Additive Manufacturing

Pellet additive manufacturing (PAM) presents a significant advancement over traditional fused filament fabrication (FFF) by addressing many of the limitations inherent in the filament-based approach. Both PAM and FFF share the fundamental principle of additive manufacturing, where objects are built layer by layer. However, PAM utilizes pellets as the raw material, which are fed through a hopper into a single-screw extrusion system, while FFF uses pre-formed filaments. This difference in raw material form and processing method provides PAM with distinct advantages, particularly in terms of cost, material flexibility, scalability, energy efficiency, environmental impact, printing volume, and productivity [38].

One of the primary advantages of PAM over FFF is the cost of raw materials. Filaments used in FFF are significantly more expensive than the same materials in pellet form. This cost difference can be attributed to the additional processing required to convert raw thermoplastics into filaments. In contrast, pellets are a more direct form of raw material, commonly used in various industrial applications, which makes them less expensive. Therefore, PAM offers a more economical solution for additive manufacturing, especially for large-scale production [39].

Material flexibility is another critical area where PAM outshines FFF. The range of materials available for filament deposition is relatively limited, which restricts the types of products that can be manufactured using FFF. PAM, on the other hand, can utilize a broader spectrum of thermoplastics, including those that are difficult or impossible to process into filaments. This increased material flexibility allows for the creation of parts with a wider array of properties, expanding the potential applications of additive manufacturing [40].

The issue of filament buckling is a notable limitation in FFF that is mitigated by the use of pellets in PAM. In FFF, if the feeding speed of the filament is too high, it can buckle, leading to print failures and reduced part quality. The pellet-based system in PAM does not suffer from this problem, as pellets are conveyed and melted directly, ensuring a more consistent and reliable extrusion process. This reliability enhances the overall efficiency and quality of the manufacturing process [41].

Energy consumption is a significant concern in FFF due to the high energy requirements of filament extrusion systems. The process of producing filaments and then melting them again during printing consumes a considerable amount of energy. PAM systems, in contrast, are generally more energy-efficient. The direct extrusion of pellets requires less energy, contributing to a more sustainable manufacturing process. This energy efficiency not only reduces operational costs but also supports environmental sustainability [42].

The environmental impact of filament production and use is another critical limitation of FFF. The production of filaments involves multiple stages of processing, which increases the overall carbon footprint of the manufacturing process. Additionally, the disposal of used or failed filaments poses environmental challenges. PAM reduces these impacts by utilizing raw pellets, which are often produced with lower environmental costs. Moreover, the ability to use recycled materials in pellet form further enhances the environmental benefits of PAM, making it an eco-friendlier alternative [43].

In terms of printing volume and productivity, PAM offers significant advantages over FFF. FFF systems are limited by the diameter and length of the filaments, which restricts the size of objects that can be printed and reduces overall productivity. PAM systems, with their ability to handle large quantities of pellets, can produce much larger objects and operate for extended periods without needing to replenish the material. This capability leads to higher printing volumes and increased productivity, making PAM suitable for large-scale manufacturing applications [44].

Pellet additive manufacturing (PAM) addresses many of the inherent limitations of fused filament fabrication (FFF) by leveraging the cost benefits, material flexibility, reliability, energy efficiency, environmental sustainability, and productivity advantages of using pellets as the raw material. These strengths make PAM a more viable and efficient option for a wide range of applications, from small-scale prototyping to large-scale industrial production. In this context, pellet additive manufacturing (PAM) has captured the attention of both researchers and industry professionals.

One notable area of investigation involves the optimization of process parameters to improve the mechanical properties of printed parts. Researchers have systematically studied the effects of extrusion temperature, print speed, and layer height on the tensile strength, flexibility, and other critical mechanical characteristics of PAM-produced objects [45]. These studies are foundational for establishing PAM as a viable manufacturing method for end-use parts in industries demanding high material performance, such as aerospace and automotive.

In addition to material properties, the surface finish of PAM-printed parts has been a focus of research. Efforts to enhance surface quality through post-processing techniques and the development of advanced nozzle designs have been reported, aiming to expand the applicability of PAM in consumer goods and other sectors where aesthetic considerations are paramount [46].

The potential of PAM for fabricating large-scale structures has also been explored, with researchers developing specialized large-format printers capable of producing components several meters in length [40]. This capability opens up new possibilities for construction and architectural applications, where the ability to print large, customized structures on-site could revolutionize traditional building methods.

Another significant avenue of research is the use of PAM for biofabrication. Studies have investigated the feasibility of using biocompatible and bioresorbable materials in pellet form for the production of scaffolds and implants tailored to individual patients [47]. This research underscores the potential of PAM in personalized medicine, where customized solutions can significantly enhance patient outcomes.

The integration of continuous fiber reinforcement in PAM processes has been examined to produce parts with enhanced strength and stiffness. By embedding fibers such as carbon or glass within the thermoplastic matrix during printing, researchers have achieved significant improvements in the structural performance of PAM parts, making them suitable for demanding engineering applications [49].

Environmental sustainability has also been a focus, with studies exploring the use of recycled materials and biodegradable polymers in PAM. The ability to directly utilize industrial plastic waste in pellet form has the potential to reduce environmental impact and promote circular economy principles within the manufacturing sector [50].

Furthermore, the development of hybrid manufacturing systems that combine PAM with subtractive processes like milling has been researched. These systems aim to leverage the advantages of both additive and subtractive methods, producing parts with complex geometries and high precision in a single setup [51].

Innovations in process control and monitoring for PAM have been another area of significant research. Implementing advanced sensors and real-time feedback mechanisms has been shown to improve the reliability and repeatability of the PAM process, essential for its adoption in industrial production environments [52].

The exploration of novel materials for PAM, including high-temperature polymers and metal-polymer composites, has expanded the technology's material palette. These materials enable the production of parts with unique properties, such as electrical conductivity or magnetic responsiveness, broadening the range of potential applications for PAM [53].

Lastly, the economic aspects of PAM have been scrutinized, with studies comparing its cost-effectiveness and efficiency against traditional manufacturing methods and other additive manufacturing technologies. These analyses are crucial for understanding the potential market impact and industrial viability of PAM [54].

The literature on pellet extrusion additive manufacturing showcases a vibrant and multidisciplinary field of research. From enhancing material properties and surface finish to exploring novel applications and materials, the works surrounding PAM are driving forward the boundaries of what is possible in additive manufacturing. As the technology continues to mature, it holds promise for revolutionizing manufacturing across a wide array of sectors.

Despite extensive research in additive manufacturing (AM), the study of hollow extrusion and the creation of variable density products by controlling the inflation rate remains largely unexplored. In traditional manufacturing, there are several examples of producing products with varying densities. For instance, injection molding can create multi-material products using dual injection methods. In casting, different material inserts can be used within the mold to achieve products with variable densities. Similarly, in automotive manufacturing, the foam density in car seats varies, with denser foam at the bottom and less dense foam for supporting the back or head.

If additive manufacturing can develop techniques to create gradient density products, it would open up a multitude of new opportunities. This capability would enable the production of components with tailored properties, optimized for specific functions and applications. The potential to control density gradients within a single build process could lead to significant advancements in various industries, including aerospace, automotive, and biomedical engineering. This innovation would mark a significant step forward, expanding the versatility and applicability of additive manufacturing technologies.

Chapter 3: Experimental Setup and Material

3.1 Material Selection

In our experiment, we utilized two distinct materials: PLA and SEBS. SEBS (Styrene-Ethylene-Butylene-Styrene) is a thermoplastic elastomer known for its flexibility, durability, and resistance to environmental factors such as UV radiation and ozone. In contrast, PLA (Polylactic Acid) is a biodegradable thermoplastic derived from renewable resources, valued for its ease of processing and environmental friendliness. The reason behind using two different types of material is to determine whether the developed methodology could be effectively applied to both materials. Additionally, we aimed to observe how changes in process parameters would impact each material, and whether these changes would produce similar results across both polymers.

PLA (Polylactic Acid) is derived from renewable resources like corn starch or sugar cane, making it biodegradable and a more environmentally friendly option compared to petroleum-based plastics. This feature is particularly appealing for applications where materials are temporarily used, such as in inflatable structures that may need to be disposed of after use. Its biodegradability ensures that it does not contribute significantly to landfill waste, aligning with sustainability goals [55,56].

Despite being biodegradable, PLA exhibits good mechanical strength and durability, which are crucial for the structural integrity of inflatable objects. PLA can maintain its form under pressure, which is necessary for inflatable applications that rely on the retention of Gas or gases. Its relatively high surface rigidity compared to other polymers also helps in maintaining the shape and structure of the inflated object.

PLA is compatible with various additives that can alter its properties to suit specific needs. For instance, plasticizers can be added to PLA to increase its flexibility, making it more suitable for inflatable applications where flexibility and elasticity are required. This compatibility allows for customization of the material properties depending on the specific requirements of the inflatable product [57].

PLA has good thermal insulation properties, which can be beneficial in inflatable applications where maintaining temperature is important. Certain grades of PLA are FDA-approved for direct contact with foods, making it a safe choice for inflatable products that may be used in food storage or transportation applications [58].

On the other hand, SEBS (Styrene-Ethylene-Butylene-Styrene) is a type of thermoplastic elastomer that combines the properties of rubber with the processing advantages of thermoplastics. Known for its excellent flexibility, high resistance to weathering, UV resistance, ozone resistance, and thermal stability, SEBS is widely used in various applications such as medical devices, automotive parts, and consumer goods. Its ability to retain elasticity and strength at a wide range of temperatures makes it particularly valuable in environments where both durability and flexibility are required. SEBS can also be easily processed using common methods like extrusion, injection molding, and blow molding, enhancing its versatility in manufacturing [59].

Overall, the choice of PLA and SEBS for our experiment was driven by their complementary properties. PLA's biodegradability and ease of processing, combined with SEBS's flexibility and durability, allowed us to thoroughly evaluate the versatility and effectiveness of our developed methodology across different types of thermoplastics and elastomers.

3.2 System Design and Specification

3.2.1 Extruder Head Design

In our experiment to extrude inflatable thermoplastic instead of solid material, we engineered a custom hot end extruder tailored to our needs. The unique design incorporated a needle, allowing the controlled flow of nitrogen gas to hollow out the extrudate. To maintain the necessary temperature for this process, we affixed a (120V, 50W) heater to the extruder. The needle was connected to an Gas pressure regulator, enabling us to fine-tune the pressure and observe the outcomes under various Gas pressure settings. This setup facilitated our exploration of creating hollow structures, offering a novel dimension to traditional 3D printing. Figure 3.1 shows the detail of extruder head.

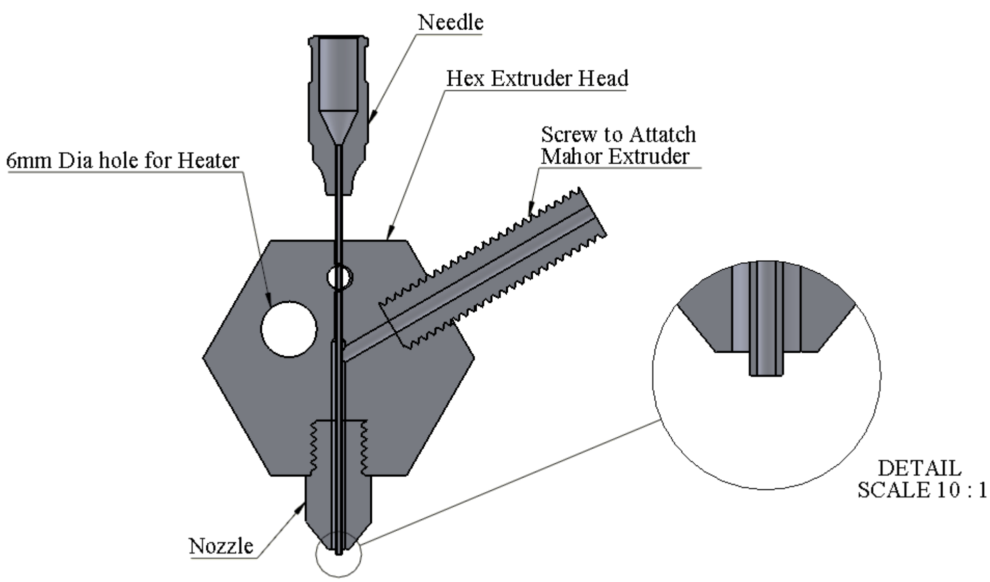

Figure 3.1 Extruder Head for Inflatable Additive Manufacturing Process.

3.2.2 Extrusion Nozzle Design

In our project to create inflatable hollow shapes, we faced the challenge of simultaneously extruding molten pellets while injecting nitrogen gas to inflate the shapes. This required a specialized nozzle design that could accommodate both functions seamlessly.

To meet this need, we decided to design a custom aluminum nozzle using 3D printing technology. This nozzle served as the interface between the extruder and the inflation process, allowing us to control both the flow of molten pellets and the injection of nitrogen gas.

One of the key considerations in the design of the nozzle was ensuring that the needle for injecting nitrogen gas remained centered within the nozzle orifice. This was crucial for maintaining precision and consistency in the inflation process. To achieve this, we added four ribs inside the nozzle, strategically positioned to guide and align the needle with the opening.

Ultimately, the customized nozzles played a critical role in our project, enabling us to precisely control the extrusion and inflation processes. By leveraging innovative design and manufacturing techniques, we were able to overcome technical challenges and achieve our goal of creating inflatable hollow shapes with accuracy and efficiency.

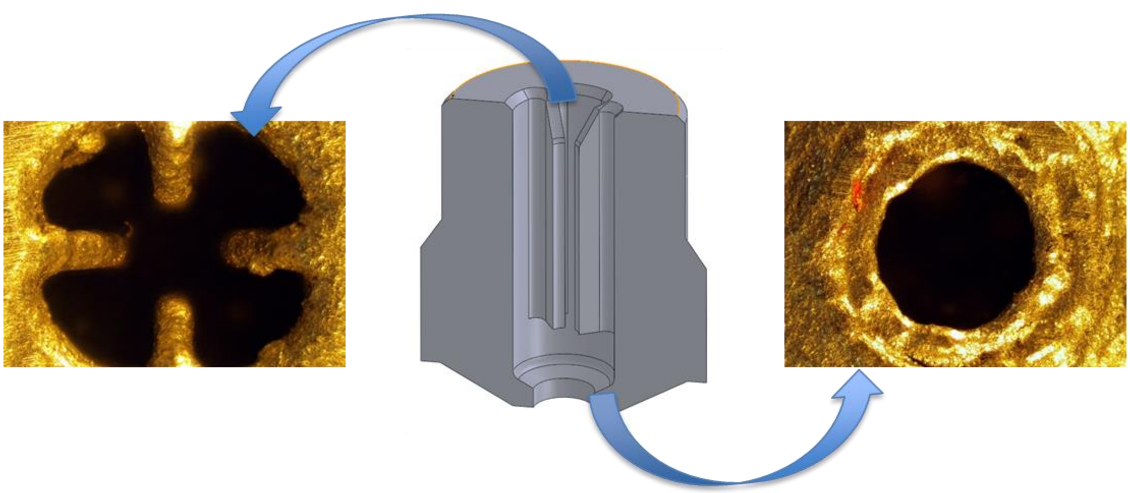

Figure 3.2. Cross-section of Extrusion Nozzle and its microscopic view.

3.2.3 Hopper Design

For the proper functioning of our experimental setup, we decided to align the Mahor pellet extruder at a 30-degree angle with the horizontal axis. This adjustment made the conventional hopper impractical for our purposes. To overcome this challenge, we designed a new hopper that would integrate with our existing setup while ensuring efficient movement of pellets to the Mahor extruder.

Our innovative solution involved crafting a hopper to maintain a vertical orientation within our setup, facilitating the natural flow of pellets to the extruder due to gravity. For the convenience during 3D printing, we opted to fabricate the hopper in two separate parts.

Leveraging the capabilities of our 3D printing lab, we printed both parts of the hopper with precision and attention to detail. With the newly designed hopper integrated into our setup, we were able to streamline the pellet feeding process to the Mahor extruder, paving the way for smoother and more efficient experimentation.

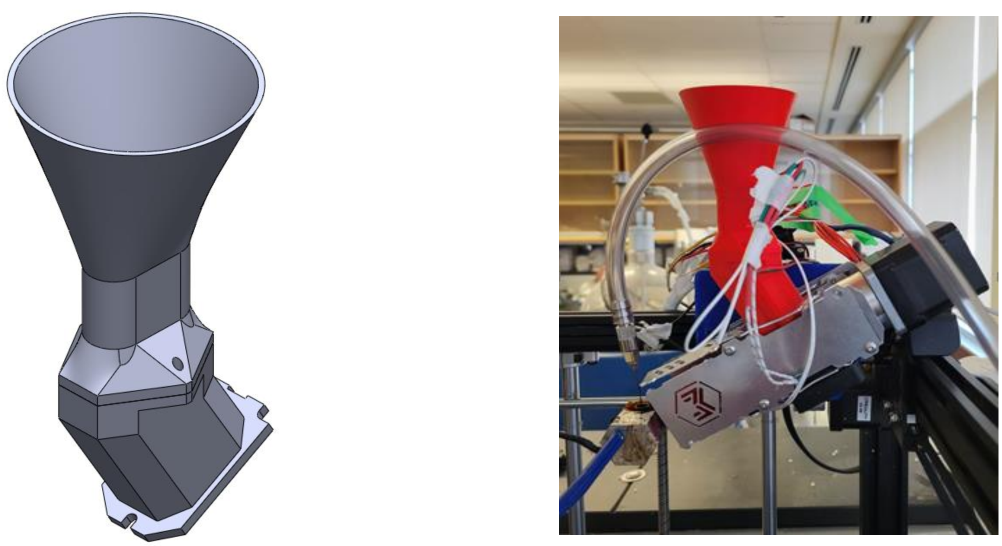

a) b)

Figure 3.3. Hopper Design a) CAD Profile b) Attached to the Mahor

3.2.4 Bracket Design

We found pellet extruder to be the most viable option for our experimental purpose. However, this decision required us to make modifications to our 3D printer's hot end zone to accommodate the Mahor pellet extruder.

To begin, we stripped down the hot end zone of the 3D printer, removing all components except for the circuit board. This circuit board served as the foundation for connecting all the components of the pellet extruder, facilitating integration into our existing setup.

In order to ensure optimal alignment and functionality, we designed a new bracket system to accommodate the pellet extruder. This system consisted of two distinct parts: one designed to securely hold the extruder in place, and the other to be affixed to the 3D printer itself. These two components were then fastened together using screws, with the extruder positioned at a precise 30-degree angle relative to the horizontal axis.

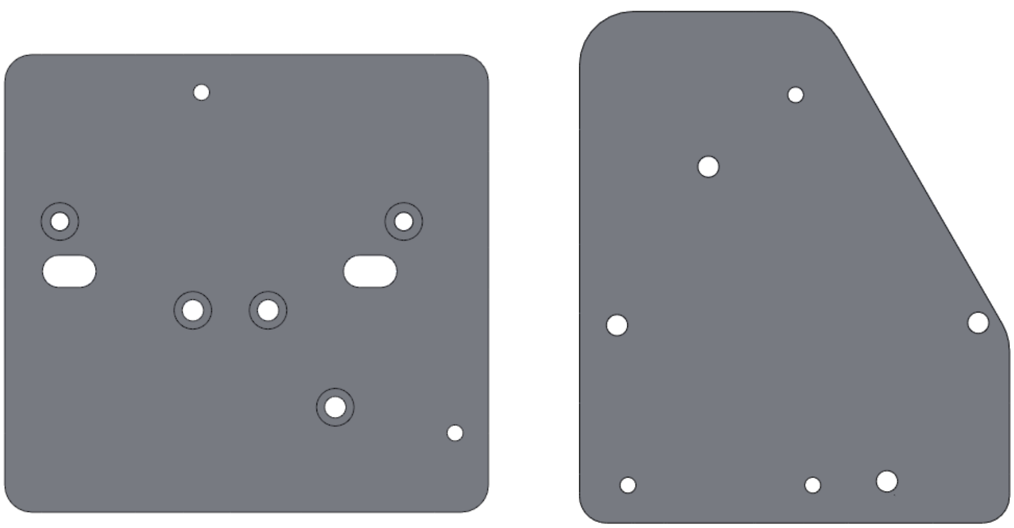

a) b)

Figure 3.4. Bracket Mechanism a) Attached to the Printer b) Attached to the Extruder

3.2.5 Mahor Pellet Extruder

Unlike traditional filament-based 3D printers, which use plastic filament as the raw material, Mahor pellet extruder uses plastic pellets or granules. The process begins with the pellets being fed into the extruder through hopper, where they are heated and melted. The molten material is then forced through the extruder nozzle, which moves along a predefined path, depositing the material layer by layer to build up the desired object.

In our experiment, we used Mahor Pellet Extruder V4 which is capable of printing a wide range of industrial material

- 3d printing standard PLA, PETG, ABS, ASA, etc.
- Low hardness flexible TPU, TPE, EVA, etc.
- Materials not available in filament
- Research and development of materials in 3D printing
- Nano fibers mixed carbon, kevlar, glass.
- Masterbatch dyes and others [60]

Figure 3.5. Mahor Pellet Extruder [61]

3.3 Assembling Components

3.3.1 Gas Pressure Regulator

A digital Gas compressor pressure regulator is used to ensure accurate pressure supplied to the system ranging from (0-160 psi). Measuring unit can be changed to bar, kgf/cm or Kpa with 0.5 unit intervals. It includes a 1/4" NPT male and female connector and a replaceable battery. Its male port is connected with the female port of the nitrogen cylinder and female port is connected with barbed hose fitting.

Figure 3.6. Air Pressure Regulator [62]

3.3.2 Barbed hose fitting

A brass made barbed hose with a straight adapter for 6mm inner diameter hose and ¼ NPT female port is used. Female port is connected with Gas pressure regulator and the straight adapter connects soft PVC tube.

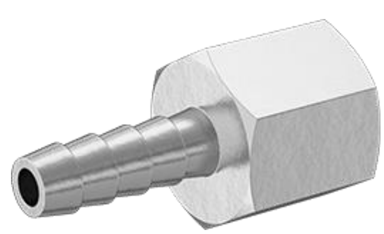

Figure 3.7. Barbed hose fitting [63]

3.3.3 Soft PVC tube

A long soft, clear PVC pipe tube of inner diameter 6mm is used to carry nitrogen gas from cylinder to the nozzle. It is very flexible to bend around an object.

Figure 3.8. Soft PVC tube [64]

3.3.4 Quick-turn plug

We used a brass made quick turn barbed plug. It one end secures the soft PVC pipe and another end connects with the luer lock of the needle.

Figure 3.9. Quick-Turn Plug [65]

3.3.5 Needle

A Stainless Steel reusable dispensing needle with a Luer lock connection is used to pass through the extrusion nozzle orifice and carry nitrogen gas to make the extrusion inflatable. The Luer lock is used to connect the quick-turn plug.

Figure 3.10. Stainless Steel Dispensing Needle [66]

3.4 Printer Connection

In our experiment, we worked with the CREALITY Ender-5 S1 3D printer. This printer has a build volume of 220x220x280mm, meaning it can create objects within those dimensions, and a printing accuracy of ±0.1mm for precise prints [67]. For the experiment's purposes, we modified the printer's hot-end to accommodate the Mahor Pellet extruder. This required crafting our bracket to securely attach the Mahor Pellet and hex extruder to the hot-end. Additionally, we added a customized hopper to guide the pellets toward the Mahor extruder during the printing process. These adjustments allowed us to explore the possibilities of using pellet-based materials in our 3D printing experiments.

3.4.1 Wiring Mahor with the 3D printer

To ensure the seamless operation of the pellet extruder with the 3D printer, we integrated it with the printer's hot-end circuit board. This integration involved connecting each electronic component of the pellet extruder to the corresponding ports on the printer's electronic board, similar to conventional extruder setups.

The hot-end circuit board featured seven connecting ports, each serving a specific function:

J1: This port is designated for connecting to the power supply, providing the necessary electrical power to the extruder system.

J2: Here, we connected the stepper motor of Mahor, specifically a Nema17 type, responsible for driving the extruder mechanism. The stepper motor typically consists of four wires: Black (A+), Green (A-), Red (B+), and Blue (B-). Stepper motor wires can be connected to the hot-end circuit board in one of the following four configurations:

Step	A+	B+	A-	B-
1	+	+	-	-
2	-	+	+	-
3	-	-	+	+
4	+	-	-	+

J3: Designed for connecting the Z sensor, which assists in positioning and calibration during the printing process.

J4 and J7: These ports are allocated for connecting fans, including the thermal shock fan and cloak fan, which help regulate the temperature and gas flow within the extruder system. These fans may operate within a voltage range of 12V to 24V.

J5: Reserved for connecting the thermistor, which monitors the temperature of the extruder system to ensure precise temperature control during printing.

J6: This port is dedicated to connecting the heater, typically a 50W, 12V, or 24V component, responsible for heating the extruder chamber to the desired temperature for melting the pellets.

Figure 3.11. Hot-end Circuit Board [68]

3.4.2 Temperature Controller

REX-C100 is a dual-line display temperature controller. The top line displays the measured temperature / Process Variable (PV) and the bottom line displays the target temperature / Set Variable (SV). The REX-C100 temperature controller is designed to be compatible with K-type thermocouples. A thermocouple is a sensor used to measure temperature, and when connected to a solid state relay (SSR), it allows precise control of a heating element. The REX-C100 ensures reliable and accurate temperature regulation, making it an essential tool for applications requiring precise thermal management.

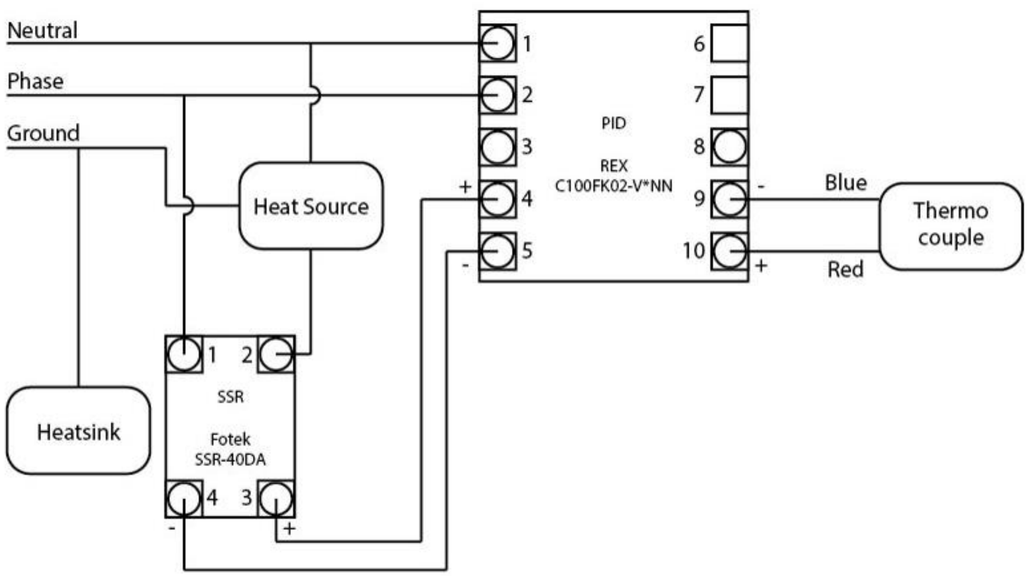

Figure 3.12. Circuit Diagram for temperature controller [69]

Chapter 4: Methodology

4.1 Process Flow

To create inflatable hollow extrudates, we implemented a meticulously crafted setup involving various components and modifications to facilitate the extrusion process.

Firstly, nitrogen gas was introduced into the system to inflate the extrudates. We utilized a cylinder to store the nitrogen gas, with a digital Gas pressure regulator connected to the outlet of the cylinder to precisely regulate the flow.

The flow of nitrogen gas was then directed through a series of components to reach the extrusion nozzle. A brass barbed hose fitting, connected to the Gas pressure regulator, served as the entry point for the gas. This fitting was linked to a soft PVC tube, which acted as the conduit for the nitrogen gas to reach the nozzle orifice of the hex extruder. The nozzle itself was equipped with a Stainless Steel Dispensing Needle, featuring a luer lock connection to ensure a secure attachment.

To maintain the integrity of the extrusion process, the hex extruder was outfitted with a 6mm threaded opening, allowing connection to the pellet extruder. The hot-end portion of the 3D printer underwent modification via a bracket system to accommodate the pellet extruder effectively. Necessary wiring connections were established to ensure the proper functioning of the pellet extruder within the printer's system.

To optimize the extrusion process further, the Mahor pellet extruder was strategically aligned at a 30-degree angle with the horizontal axis, enhancing the convenience of the experiment. This alignment necessitated the design of a new hopper to ensure the pellets flowed smoothly to the extruder, utilizing gravitational force.

The journey of the molten pellet from the hex extruder to the nozzle outlet was carefully monitored to maintain its temperature throughout. An external heater was affixed to the hex extruder, with temperature control facilitated by a temperature controller. This comprehensive setup and meticulous attention to detail enabled us to achieve the controlled extrusion of inflatable hollow extrudates, showcasing the synergy of innovative design and advanced technology in additive manufacturing.

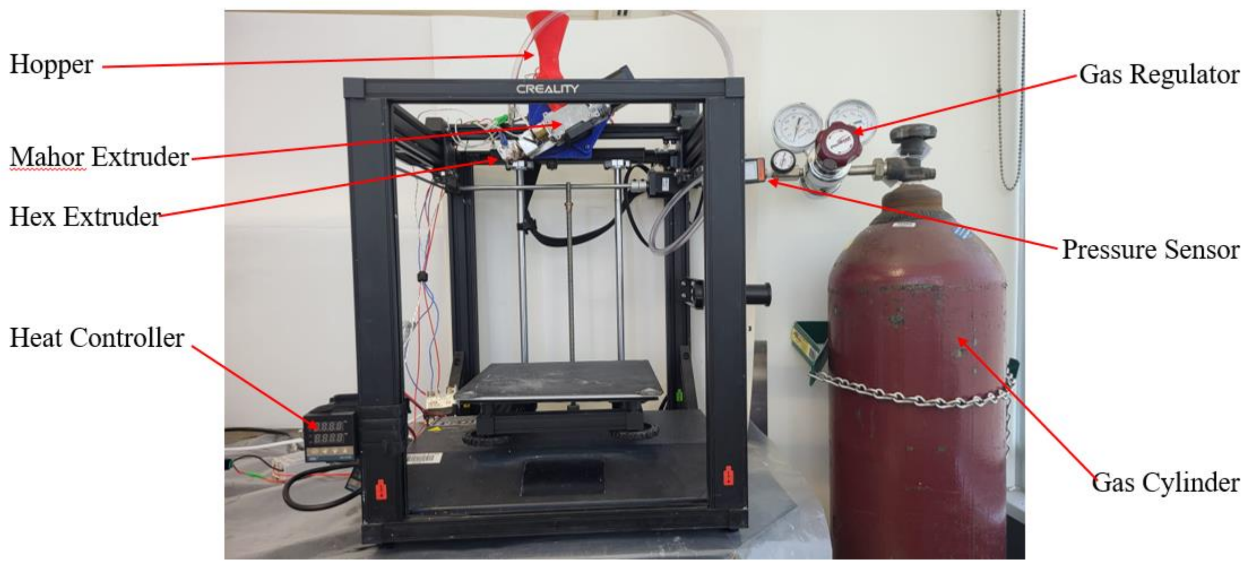

Figure 4.1 Process Setup

4.2 G Code Generation

To generate Gcode for 3D printing an innovative open-source software called FullControl GCode Designer (https://fullcontrolgcode.com/)is used. This method allowed us to define every aspect of the print-path, at each point along the way. Unlike traditional methods that rely on computer-aided design (CAD), STL files, or slicing software, FullControl generates machine control code (GCode) directly, eliminating the need for programming skills.

Excel serves as the user interface for FullControl, which is developed in Visual Basic. We used Repetier Host, a versatile and user-friendly slicing software widely used in the field of 3D printing to preview and edit out GCode. The software provides a visual preview of the sliced model, allowing it to inspect each layer and identify any potential issues such as overhangs, gaps, or intersections. This preview helped us ensure the model was sliced correctly before initiating the printing process. Repetier Host also allows to editing of the generated G-code, which contains instructions for the 3D printer. Now this generated GCode is saved in a memory card, and then the card is connected to the printer for printing.

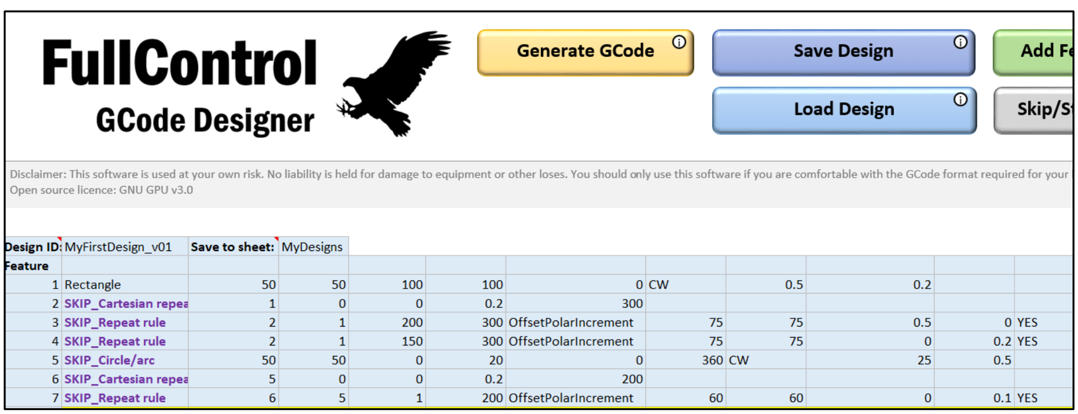

Figure 4.2 Excel interface for Full Control to Generate GCode.

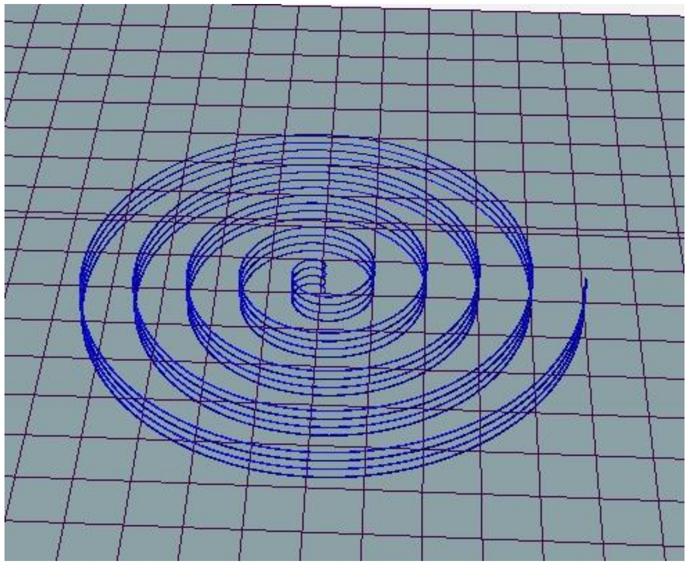

Figure 4.3 GCode Preview in Repetier Host software

4.3 Sample Generation

4.3.1 Sample Preparation for Microscopic Image

In the initial phase of our research, we aimed to create an inflatable extrudate by adjusting various process parameters, including temperatures, flow rates, and Gas pressure. We commenced our experiment by selecting two different temperatures: 205 °C and 220 °C for PLA and 220 °C and 230 °C for SEBS. For each temperature, we identified the maximum and minimum values for other parameters and produced samples using various combinations of these values.

For each combination of parameters, we collected five freely extruded samples and calculated the average value of the volumetric flow rate. We changed the volumetric flow rate by changing the extrusion speed. Subsequently, we took small cross-sections of each sample and observed them under a microscope. We measured the outer diameter, inner diameter, and shell thickness at different positions and calculated the average values for each.

Our next step was to analyze the relationship between the process parameters and the dimensions of the extrudates. Understanding this relationship is crucial as it will enable us to predict and assume process parameter combinations to achieve desired extrudate dimensions in future experiments.

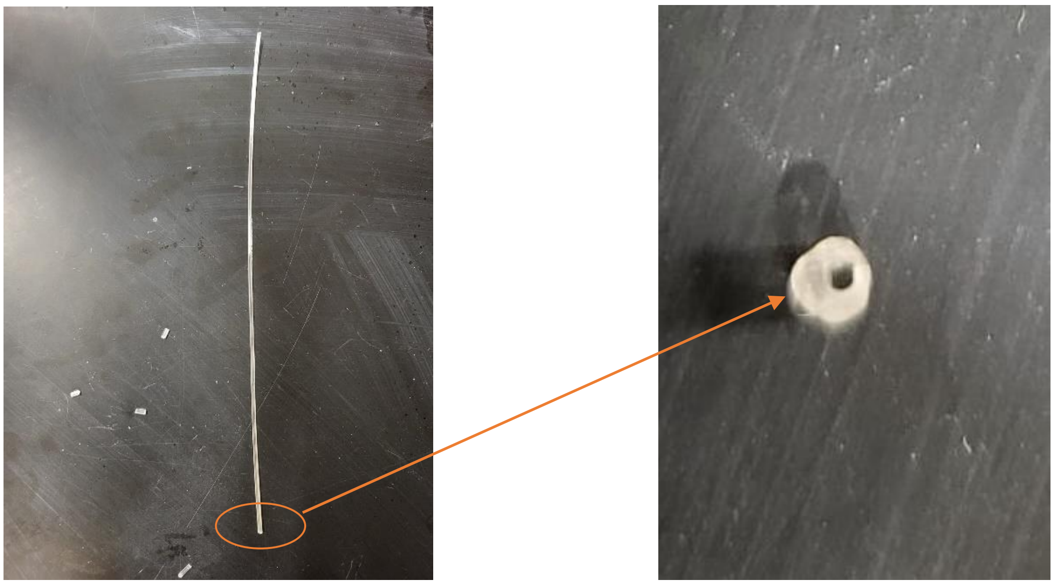

a) b)

Figure 4.4 a) Extruded Sample b) Cross-Section of Extruded Sample

In our experiment, we conducted a comprehensive microscopic observation of the inflatable thermoplastic extrudates produced using a major pellet extruder, specifically focusing on two distinct materials: PLA and SEBS. This observation was performed under various process combinations of temperature, Gas pressure, and extrusion speed. The primary objective was to measure and analyze critical dimensions such as outer diameter, core diameter, and shell thickness.

To achieve this, we first prepared samples of PLA and SEBS by extruding them using a pellet extruder. After the extrusion process, the samples were subjected to microscopic observation. This involved using high-resolution optical and electron microscopy to capture detailed images of the cross-sectional structure of the inflatable extrudates. These microscopic techniques allowed us to examine the internal and external features of the samples with high precision. For each sample, we measured the outer diameter, core diameter, and shell thickness. These measurements were taken at multiple points along the length of the extrudates to ensure accuracy and reliability. The outer diameter was determined by measuring the overall width of the sample, while the core diameter was measured by examining the inner hollow section of the extrudate. The shell thickness was calculated by subtracting the core diameter from the outer diameter and dividing by two, providing an average value for the thickness of the material's shell.

The data collected from these microscopic observations and measurements were systematically analyzed to draw correlations between the process parameters and the resulting dimensions of the extrudates. This analysis provided valuable insights into the behavior of PLA and SEBS during the extrusion process and helped us understand the specific conditions that produce the best results for each material.

Figure 4.5 OMAX Optical Microscope

4.3.2 Cylindrical Sample Printing

In the initial phase of our experiment, we collected extruded samples under different process parameters and observed their various dimensions. With this foundational data, we printed objects and verified whether they match the measurements obtained in the initial stage of the experiment. Specifically, we have decided to print spiral cylindrical objects.

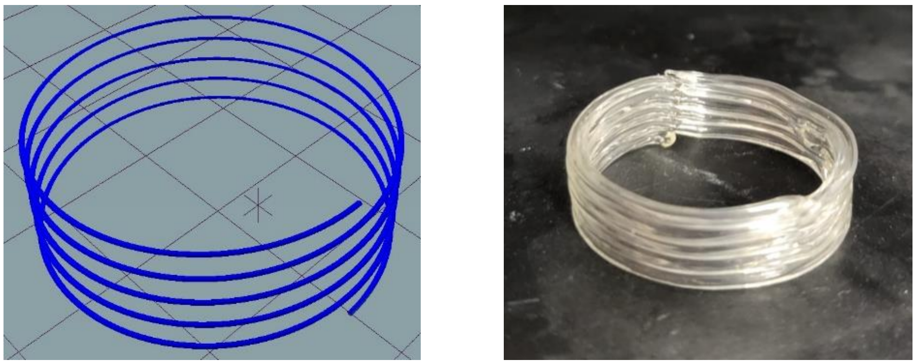

a) b)

Figure 4.6 Spiral Cylindrical Printed Part a) Print Part Preview b) Printed Part

We also printed multi-layer cylindrical object, layers in both vertical and horizontal direction.

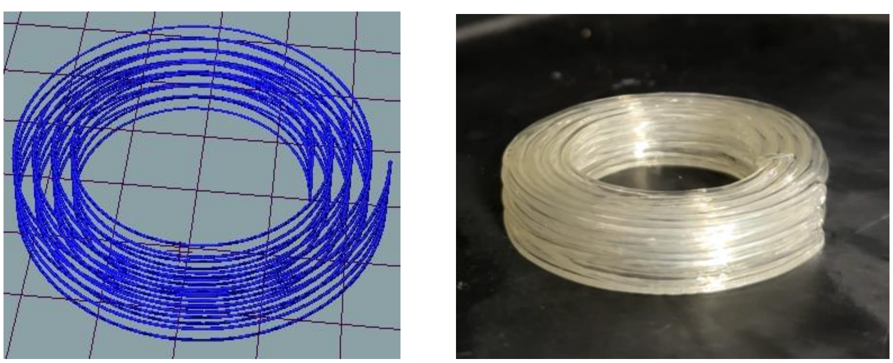

a) b)

Figure 4.7 Spiral multi-layer Cylindrical Printed Part a) Print-Path Preview b) Printed Part

4.3.3 Printing Sample with Different density in different portions

The primary objective of our experiment was to develop a body with varying densities in different sections. To achieve this, we divided the product into two portions: one with solid layers (no inflation) and the other with inflatable layers. This approach allows us to create an object with distinct densities in each section.

We printed an object with one half being semicircular and the other half being C-shaped. The printing process was as follows:

We began by printing two solid layers in the C-shaped section, each with a layer height of 1 mm. Next, we continued printing into the semicircular portion, where we introduced inflation, achieving a layer height of 2 mm. After printing one inflatable layer in the semicircular portion, we returned to printing solid layers.

Following this method, we printed a total of eight solid layers in the C-shaped half and four inflatable layers in the semicircular half. This process successfully created an object with two distinct densities in its different portions, fulfilling the main objective of our experiment. We achieved the inflation by passing nitrogen gas and it was controlled manually.

Figure 4.8. Printed Sample with different Densities a) Print Path Preview b) Isometric View c) Front View

Chapter 5: Analytical Modeling

5.1 Flow Through an Annular Die

To derive the annular flow equation for a polymer under the influence of gravity, we need to consider the effect of gravitational force in addition to the pressure gradient driving the flow. This analysis will involve the balance of forces in the radial and axial directions within the annulus.

Assumptions

1. Steady flow: The flow is stable over time, $\frac{\partial v_z}{\partial t} = 0$
2. Incompressible flow, ρ, μ= Constant, Laminar flow.
3. For fully developed flow, $\frac{\partial P}{\partial z} = Constant$
4. There is only one nonzero velocity component, namely that in the direction of flow, v_z. Thus, $v_r = v_\theta = 0$.
5. The axial velocity is independent of the angular location; that is, $\frac{\partial v_z}{\partial \theta} = 0$.
6. The fluid flows between two concentric cylinders with inner radius R_i and outer radius R_o.

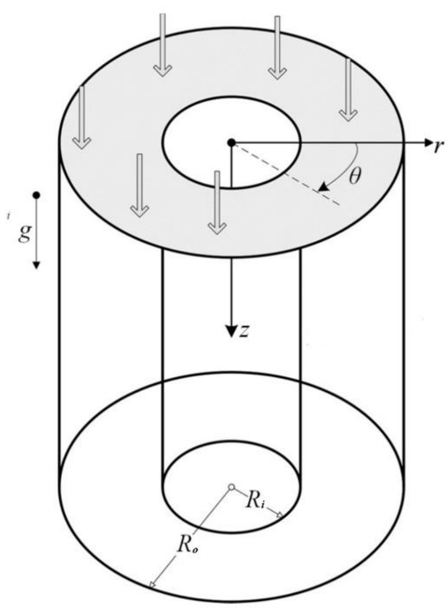

Figure 5.1 Flow Geometry through an Annular Die

To analyze the situation, again start from the continuity equation

$$\frac{1}{r}\frac{\partial(rv_r)}{\partial r}+\frac{1}{r}\frac{\partial v_\theta}{\partial\theta}+\frac{\partial v_z}{\partial z}=0$$

[70]

as, $v_r = v_\theta = 0$, it reduces the equation to:

$$\frac{\partial v_z}{\partial z}=0$$

verifying that v_z is independent of distance from the inlet, and that the velocity profile $v_z = v_z(r)$ appears the same for all values of z.

There are again three momentum balances, one for each of the r, θ, and z directions. If explored, the first two of these would ultimately lead to the pressure variation with r and θ at any cross section, which is of little interest in this problem.

z component:

$$\rho\left(\frac{\partial v_z}{\partial t}+vr\frac{\partial z}{\partial r}+\frac{v_\theta}{r}\frac{\partial v_z}{\partial\theta}+v_z\ \frac{\partial v_z}{\partial z}\right)=\rho g_z-\frac{\partial P}{\partial z}+\mu\left\{\frac{1}{r}\frac{\partial}{\partial r}\left(r\frac{\partial v_z}{\partial r}\right)+\frac{1}{r^2}\ \frac{\partial^2 v_z}{\partial\theta^2}+\frac{\partial^2 v_z}{\partial z^2}\right\}$$

[70]

Now,

1. $v_r = v_\theta = 0$, (assumption 4)
2. $\frac{\partial v_z}{\partial t}=0$, (assumption 1)
3. $\frac{\partial v_z}{\partial z}=0$, (continuity equation)
4. $\frac{\partial v_z}{\partial\theta}=0$, (assumption 5), reduces the equation 3 into,

$$\mu\left\{\frac{1}{r}\,\frac{\partial}{\partial r}\,\left(r\frac{\partial v_z}{\partial r}\right)\right\} = \frac{\partial P}{\partial \mathrm{z}} - \rho g_z$$

$$\mu\left\{\frac{1}{r}\,\frac{\partial}{\partial r}\,\left(r\frac{\partial v_z}{\partial r}\right)\right\} = \frac{\partial P}{\partial \mathrm{z}} - \rho g$$

$$\frac{\partial}{\partial r}\left(r\frac{\partial v_z}{\partial r}\right) = \frac{r}{\mu}\left(\frac{\partial P}{\partial \mathrm{z}} - \rho g\right)$$

Integrating

$$r\frac{\partial v_z}{\partial r} = \frac{r^2}{2\mu}\left(\frac{\partial P}{\partial \mathrm{z}} - \rho g\right) + c1$$

$$\frac{\partial v_z}{\partial r} = \frac{r}{2\mu}\left(\frac{\partial P}{\partial \mathrm{z}} - \rho g\right) + c1$$

Integrating

$$v_z = \frac{r}{2\mu}\left(\frac{\partial P}{\partial \mathrm{z}} - \rho g\right) + c1lnr + c2$$

The two constants may be evaluated by applying the boundary conditions of zero velocity at the inner and outer walls,

$$v_z = -\frac{r^2}{4\mu}\left(-\frac{\partial P}{\partial \mathrm{z}} + \rho g\right) + c1lnr + c2$$

$r = R_i$: $v_z = 0$,

$$0 = -\frac{R_i^2}{4\mu}\left(-\frac{\partial P}{\partial \mathrm{z}} + \rho g\right) + c1lnR_i + c2$$

$r = R_o$: $v_z = 0$

$$0 = -\frac{R_0^2}{4\mu}\left(-\frac{\partial P}{\partial \mathrm{z}} + \rho g\right) + c1lnR_o + c2$$

$$-\frac{R_0^2}{4\mu}\left(-\frac{\partial P}{\partial \mathrm{z}} + \rho g\right) + c1lnR_o = -\frac{R_i^2}{4\mu}\left(-\frac{\partial P}{\partial \mathrm{z}} + \rho g\right) + c1lnR_i$$

$$\frac{1}{4\mu}\left(-\frac{\partial P}{\partial z}+\ \rho g\right)(R_0^2-R_i^2)=c1ln\frac{R_0}{R_i}$$

$$c1=\frac{1}{4\mu}\left(-\frac{\partial P}{\partial z}+\ \rho g\right)\frac{(R_0^2-R_i^2)}{ln\frac{R_0}{R_i}}$$

Now

$$0=-\frac{R_i^2}{4\mu}\left(-\frac{\partial P}{\partial z}+\ \rho g\right)+\frac{1}{4\mu}\left(-\frac{\partial P}{\partial z}+\ \rho g\right)\frac{(R_0^2-R_i^2)}{ln\frac{R_0}{R_i}}lnR_i+\ c2$$

$$c2=\frac{R_i^2}{4\mu}\left(-\frac{\partial P}{\partial z}+\ \rho g\right)-\frac{1}{4\mu}\left(-\frac{\partial P}{\partial z}+\ \rho g\right)\frac{(R_0^2-R_i^2)}{ln\frac{R_0}{R_i}}lnR_i$$

$$c2=\frac{1}{4\mu}\left(-\frac{\partial P}{\partial z}+\ \rho g\right)\left(R_i^2-\frac{(R_0^2-R_i^2)}{ln\frac{R_0}{R_i}}lnR_i\right)$$

Substituting c_1 and c_2 into the velocity profile equation:

$$v_z=-\frac{r^2}{4\mu}\left(-\frac{\partial P}{\partial z}+\ \rho g\right)+c1lnr+\ c2$$

$$v_z=-\frac{r^2}{4\mu}\left(-\frac{\partial P}{\partial z}+\ \rho g\right)+\frac{1}{4\mu}\left(-\frac{\partial P}{\partial z}+\ \rho g\right)\frac{(R_0^2-R_i^2)}{ln\frac{R_0}{R_i}}lnr$$

$$+\ \frac{1}{4\mu}\left(-\frac{\partial P}{\partial z}+\ \rho g\right)\left(R_i^2-\frac{(R_0^2-R_i^2)}{ln\frac{R_0}{R_i}}lnR_i\right)$$

$$v_z=\frac{1}{4\mu}\left(-\frac{\partial P}{\partial z}+\ \rho g\right)\left[R_i^2-r^2+\frac{(R_0^2-R_i^2)}{ln\frac{R_0}{R_i}}ln\frac{r}{R_i}\right]$$

5.2 Flow Rate Calculation:

The volumetric flow rate Q is obtained by integrating the velocity profile $v_z(r)$ over the cross-sectional area A of the annulus.

$$Q = \int_A v_z(r)dA$$

In cylindrical coordinates, the differential area element dA is $2\pi rdr$.

$$Q = \int_{Ri}^{Ro} v_z(r)\, 2\pi r\, dr$$

$$Q = \int_{Ri}^{Ro} [\frac{1}{4\mu}\left(-\frac{\partial P}{\partial z} + \rho g \right)\left[R_i^2 - r^2 + \frac{(R_0^2 - R_i^2)}{ln\frac{R_0}{R_i}} ln\frac{r}{R_i}\right] 2\pi rdr$$

$$Q = \frac{1}{4\mu}\left(-\frac{\partial P}{\partial z} + \rho g\right).2\pi\left[-\int_{Ri}^{Ro} r^3 dr + R_i^2\int_{R_i}^{R_o} rdr + \frac{\left(R_o{}^2 - R_i{}^2\right)}{\ln\left(\frac{R_o}{R_i}\right)}\int_{R_i}^{R_o} rlnrdr\right.$$

$$\left. - \frac{\left(R_o{}^2 - R_i{}^2\right)}{\ln\left(\frac{R_o}{R_i}\right)} lnR_i \int_{R_i}^{R_o} rdr\right]$$

$$Q = \frac{1}{4\mu}\left(-\frac{\partial P}{\partial z} + \rho g\right)2\pi\left[-\frac{1}{4}(R_o^4 - R_i^4) + \frac{R_i^2}{2}(R_o^2 - R_i^2) - \frac{\left(R_o{}^2 - R_i{}^2\right)}{\ln\left(\frac{R_o}{R_i}\right)} lnR_i\left(\frac{R_o^2 - R_i^2}{2}\right)\right.$$

$$\left. + \frac{\left(R_o{}^2 - R_i{}^2\right)}{\ln\left(\frac{R_o}{R_i}\right)}\left(\frac{R_o^2 lnR_o}{2} - \frac{R_i^2 lnR_i}{2} - \frac{R_o^2}{4} + \frac{R_i^2}{4}\right)\right]$$

$$Q = \frac{1}{4\mu}\left(-\frac{\partial P}{\partial z} + \rho g\right) 2\pi \left[-\frac{1}{4}(R_o^4 - R_i^4) + \frac{R_i^2}{2}(R_o^2 - R_i^2) - \frac{1}{2}\frac{\left({R_o}^2 - {R_i}^2\right)}{\ln\left(\frac{R_o}{R_i}\right)} R_o^2 lnR_i \right.$$

$$\left. + \frac{\left({R_o}^2 - {R_i}^2\right)}{\ln\left(\frac{R_o}{R_i}\right)}\frac{R_o^2 lnR_o}{2} - \frac{\left({R_o}^2 - {R_i}^2\right)}{\ln\left(\frac{R_o}{R_i}\right)}\left(\frac{R_o^2 - R_i^2}{4}\right)\right]$$

$$Q = \frac{1}{4\mu}\left(-\frac{\partial P}{\partial z} + \rho g\right) 2\pi \frac{1}{4}(R_o^2 - R_i^2)\left(-R_o^2 - R_i^2 + 2R_i^2 - \frac{2R_o^2 lnR_i}{\ln\left(\frac{R_o}{R_i}\right)} + \frac{2R_o^2 lnR_i}{\ln\left(\frac{R_o}{R_i}\right)} - \frac{\left({R_o}^2 - {R_i}^2\right)}{\ln\left(\frac{R_o}{R_i}\right)}\right)$$

$$Q = \frac{\pi(R_o^2 - R_i^2)}{8\mu}\left(-\frac{\partial P}{\partial z} + \rho g\right)\left(-(R_o^2 - R_i^2) - \frac{2R_o^2 lnR_i}{\ln\left(\frac{R_o}{R_i}\right)} + \frac{2R_o^2 lnR_o}{\ln\left(\frac{R_o}{R_i}\right)} - \frac{\left({R_o}^2 - {R_i}^2\right)}{\ln\left(\frac{R_o}{R_i}\right)}\right)$$

$$Q = \frac{\pi(R_o^2 - R_i^2)}{8\mu}\left(-\frac{\partial P}{\partial z} + \rho g\right)\left(-(R_o^2 - R_i^2) + \frac{2R_o^2 \ln(\frac{R_o}{R_i})}{\ln\left(\frac{R_o}{R_i}\right)} - \frac{\left({R_o}^2 - {R_i}^2\right)}{\ln\left(\frac{R_o}{R_i}\right)}\right)$$

$$Q = \frac{\pi(R_o^2 - R_i^2)}{8\mu}\left(-\frac{\partial P}{\partial z} + \rho g\right)\left(-(R_o^2 - R_i^2) + 2R_o^2 - \frac{\left({R_o}^2 - {R_i}^2\right)}{\ln\left(\frac{R_o}{R_i}\right)}\right)$$

$$Q = \frac{\pi(R_o^2 - R_i^2)}{8\mu}\left(-\frac{\partial P}{\partial z} + \rho g\right)\left(R_o^2 + R_i^2 - \frac{\left({R_o}^2 - {R_i}^2\right)}{\ln\left(\frac{R_o}{R_i}\right)}\right)$$

5.3 Shear Rate Calculation through an annular die

The shear rate, often denoted by γ˙, is a measure of the rate at which a fluid is deformed due to shear forces. It quantifies how quickly adjacent layers of fluid move with respect to each other. In simpler terms, it represents the velocity gradient perpendicular to the direction of the shear force.

Mathematical Definition

The shear rate in a flow field is defined as the derivative of the velocity with respect to the position perpendicular to the flow direction:

$$\dot{\gamma}(r) = \frac{dv_z(r)}{dr}$$

Where:

- v_z is the velocity in the flow direction.
- r is the position perpendicular to the flow direction.

$$v_z = \frac{1}{4\mu}\left(-\frac{\partial P}{\partial z} + \rho g\right)\left[R_i^2 - r^2 + \frac{(R_0^2 - R_i^2)}{ln\frac{R_0}{R_i}} ln\frac{r}{R_i}\right]$$

$$v_z = \frac{d}{dr}\left(\frac{1}{4\mu}\left(-\frac{\partial P}{\partial z} + \rho g\right)\left[R_i^2 - r^2 + \frac{(R_0^2 - R_i^2)}{ln\frac{R_0}{R_i}} ln\frac{r}{R_i}\right]\right)$$

$$\dot{\gamma}(r) = \left(\frac{1}{4\mu}\left(-\frac{\partial P}{\partial z} + \rho g\right)\left[-2r + \frac{(R_0^2 - R_i^2)}{rln\frac{R_0}{R_i}}\right]\right)$$

Now,

$$Q = \frac{\pi(R_o^2 - R_i^2)}{8\mu}\left(-\frac{\partial P}{\partial z} + \rho g\right)\left(R_o^2 + R_i^2 - \frac{({R_o}^2 - {R_i}^2)}{\ln\left(\frac{R_o}{R_i}\right)}\right)$$

$$\left(-\frac{\partial P}{\partial \mathrm{z}}+\ \rho g\ \right)=\ \frac{8Q\mu}{\pi\left({R_o}^2-{R_i}^2\right)\left[R_o^2+R_i^2-\frac{\left(\ {R_o}^2-{R_i}^2\right)}{\ln\left(\frac{R_o}{R_i}\right)}\right]}$$

$$\dot{\gamma}(r)=\left(\frac{2Q}{\pi({R_o}^2-{R_i}^2)[R_o^2+R_i^2-\frac{\left(\ {R_o}^2-{R_i}^2\right)}{\ln\left(\frac{R_o}{R_i}\right)}]}\right)\left[-2r+\frac{(R_0^2-R_i^2)}{rln\frac{R_0}{R_i}}\right]$$

5.4 Annular Flow (Inner profile cylindrical but outer profile conical)

For annular flow where the inner profile is cylindrical and the outer profile is conical, we need to consider the geometry of the system. The inner radius remains constant (Ri), but the outer radius changes linearly with z, the axial coordinate.

Let's define the outer radius $R_o(z)$ as a linear function of z:

$$R_o(z)=R_{o0}+kz$$

where:

- R_{o0} is the outer radius at $z=0$
- k is the slope of the conical profile.

We start from the general form of the Navier-Stokes equation for incompressible, steady, and fully developed flow in cylindrical coordinates for an annulus. The velocity profile in the z-direction (axial direction) is given by the solution to the governing differential equation, considering the new boundary conditions.

The governing differential equation for steady, incompressible flow in the z-direction in cylindrical coordinates is:

z component:

$$\rho\left(\frac{\partial v_{\mathrm{z}}}{\partial \mathrm{t}}+vr\frac{\partial \mathrm{z}}{\partial \mathrm{r}}+\frac{v_\theta}{r}\frac{\partial v_{\mathrm{z}}}{\partial \theta}+v_z\ \frac{\partial v_{\mathrm{z}}}{\partial \mathrm{z}}\right)=\rho g_z-\frac{\partial P}{\partial \mathrm{z}}+\mu\left\{\frac{1}{r}\frac{\partial}{\partial r}\left(r\frac{\partial v_z}{\partial r}\right)+\frac{1}{r^2}\ \frac{\partial^2 v_z}{\partial \theta^2}+\frac{\partial^2 v_z}{\partial z^2}\right\}$$

Now,

1. $v_r = v_\theta = 0$, (assumption 4)
2. $\frac{\partial v_{\mathrm{z}}}{\partial \mathrm{t}}=0$, (assumption 1)

3. $\frac{\partial v_z}{\partial z} = 0$, (continuity equation)

4. $\frac{\partial v_z}{\partial \theta} = 0$, (assumption 5)

$$\mu\left\{\frac{1}{r}\frac{\partial}{\partial r}\left(r\frac{\partial v_z}{\partial r}\right)\right\} = \frac{\partial P}{\partial z} - \rho g_z$$

The geometry and coordinate system used to model the flow field are shown. (The z coordinate is directed vertically upward; as a consequence, $g_z = -g$

$$\mu\left\{\frac{1}{r}\frac{\partial}{\partial r}\left(r\frac{\partial v_z}{\partial r}\right)\right\} = \frac{\partial P}{\partial z} + \rho g$$

For the given boundary conditions:

- At $r=R_i$, $v_z=0$.
- At $r=R_o(z)=R_{o0}+kz$, $v_z=0$. [k is the slope of the conical profile]

The general solution to the differential equation is:

$$v_z = -\frac{r^2}{4\mu}\left(-\frac{\partial P}{\partial z} + \rho g\right) + A ln r + B$$

Boundary Condition: $r= R_i$, $v_z= 0$

$$0 = -\frac{{R_i}^2}{4\mu}\left(-\frac{\partial P}{\partial z} + \rho g\right) + A ln R_i + B$$

Boundary Condition: $r= R_o = R_{o0}+kz$, $v_z= 0$

$$0 = -\frac{(R_{o0}+kz)^2}{4\mu}\left(-\frac{\partial P}{\partial z} + \rho g\right) + A ln(R_{o0}+kz) + B$$

$$-\frac{{R_i}^2}{4\mu}\left(-\frac{\partial P}{\partial z} + \rho g\right) + A ln R_i + B = -\frac{(R_{o0}+kz)^2}{4\mu}\left(-\frac{\partial P}{\partial z} + \rho g\right) + A ln(R_{o0}+kz) + B$$

$$A(ln(R_{o0}+kz) - ln R_i) = \frac{1}{4\mu}\left(-\frac{\partial P}{\partial z} + \rho g\right)\left[(R_{o0}+kz)^2 - {R_i}^2\right]$$

$$A\left(ln\frac{(R_{o0}+kz)}{R_i}\right) = \frac{1}{4\mu}\left(-\frac{\partial P}{\partial z} + \rho g\right)\left[(R_{o0}+kz)^2 - {R_i}^2\right]$$

$$A=\frac{1}{4\mu}\left(-\frac{\partial P}{\partial z}+\rho g\right)\frac{\left[\left(R_{o0}+kz\right)^2-{R_i}^2\right]}{ln\frac{(R_{o0}+kz)}{R_i}}$$

Now,

$$0=-\frac{{R_i}^2}{4\mu}\left(-\frac{\partial P}{\partial z}+\rho g\right)+AlnR_i+B$$

$$0=-\frac{{R_i}^2}{4\mu}\left(-\frac{\partial P}{\partial z}+\rho g\right)+\frac{\frac{1}{4\mu}\left(-\frac{\partial P}{\partial z}-\rho g\right)\left[(R_{o0}+kz)^2-{R_i}^2\right]}{ln\frac{(R_{o0}+kz)}{R_i}}lnR_i+B$$

$$B=\frac{1}{4\mu}\left(-\frac{\partial P}{\partial z}+\rho g\right)\left({R_i}^2-\frac{\left[(R_{o0}+kz)^2-{R_i}^2\right]}{ln\frac{(R_{o0}+kz)}{R_i}}lnR_i\right)$$

$$v_z=-\frac{r^2}{4\mu}\left(-\frac{\partial P}{\partial z}+\rho g\right)+\frac{1}{4\mu}\left(-\frac{\partial P}{\partial z}-\rho g\right)\frac{\left[\left(R_{o0}+kz\right)^2-{R_i}^2\right]}{ln\frac{(R_{o0}+kz)}{R_i}}lnr$$

$$+\frac{1}{4\mu}\left(-\frac{\partial P}{\partial z}+\rho g\right)\left({R_i}^2-\frac{\left[(R_{o0}+kz)^2-{R_i}^2\right]}{ln\frac{(R_{o0}+kz)}{R_i}}lnR_i\right)$$

$$v_z=\frac{1}{4\mu}\left(-\frac{\partial P}{\partial z}+\rho g\right)\left({R_i}^2-r^2+\frac{\left[\left(R_{o0}+kz\right)^2-{R_i}^2\right]}{ln\frac{(R_{o0}+kz)}{R_i}}lnr-\frac{\left[(R_{o0}+kz)^2-{R_i}^2\right]}{ln\frac{(R_{o0}+kz)}{R_i}}lnR_i\right)$$

$$v_z=\frac{1}{4\mu}\left(-\frac{\partial P}{\partial z}+\rho g\right)\left({R_i}^2-r^2+\frac{\left[\left(R_{o0}+kz\right)^2-{R_i}^2\right]}{ln\frac{(R_{o0}+kz)}{R_i}}\ln\frac{r}{R_i}\right)$$

Now, the pressure gradient varies along the length of the cone, we can express it as:

$$v_z = \frac{1}{4\mu}\left(-\frac{\partial P}{\partial z}(z) + \rho g\right)\left(R_i{}^2 - r^2 + \frac{\left[\left(R_{o0} + kz\right)^2 - R_i{}^2\right]}{ln\,\frac{(R_{o0} + kz)}{R_i}}\ln\frac{r}{R_i}\right)$$

This equation describes the velocity profile of fluid flowing through an annulus with a cylindrical inner profile and a conical outer profile, incorporating the effects of pressure gradient and gravitational force.

5.5 Comparative Analysis

In the figure below, we can observe the cross-section of the nozzle used in our experiment. The nozzle is designed to facilitate the flow of molten plastic around a central needle that carries nitrogen gas. This setup results in the polymer flowing as an annular flow around the needle. The nozzle consists of two distinct regions: a cylindrical section and a conical section. For both section mathematical equation for velocity, and flow rate is derived above.

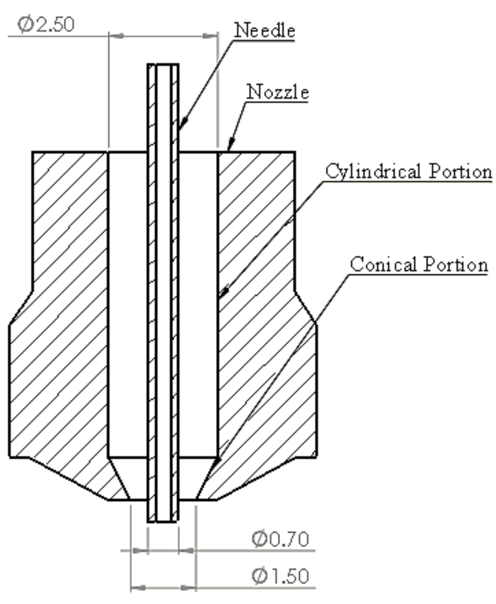

Figure 5.2. Cross-section of the nozzle used

For the sake of calculation, we will assume few values because we could not measure them. As we could not measure pressure we will consider three different pressure gradient ($\frac{\partial P}{\partial z}$=1 MPa/mm, 2 MPa/mm, and 3 MPa/mm), viscosity (μ) of PLA is calculate from Figure 5.3. We assumed our viscosity (μ) is 70 Pa.s. as we conducted our experiment in 205°C and 220°C.

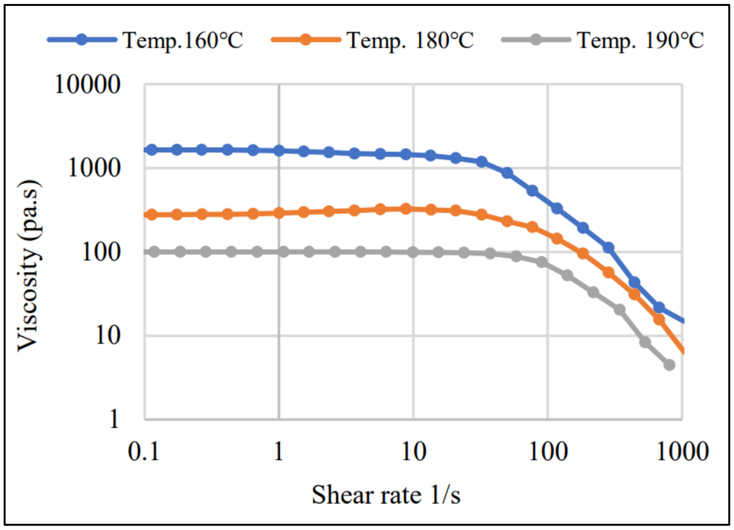

Figure 5.3. Viscosity as a function of temperature and shear rate for Amorphous PLA [69]

Now we will calculate the velocity for the cylindrical portion of the nozzle for three different pressure gradients. The outer diameter of the needle was 0.70mm and the inner diameter of the nozzle in the cylindrical portion was 2.5mm. For each pressure at a different radial point between the needle outer diameter and nozzle inner diameter velocity was calculated and recorded shown in Table 5.1. Later we plotted those values into a graph Figure 5.4.

$$v_z = \frac{1}{4\mu}\left(-\frac{\partial P}{\partial z} + \rho g\right)\left[R_i^2 - r^2 + \frac{(R_0^2 - R_i^2)}{ln\frac{R_0}{R_i}} ln\frac{r}{R_i}\right]$$

Table 5.1 Velocity in the cylindrical zone for different assumed pressure gradient

r(mm)	r (relative)	V_z (mm/s)		
		$\frac{\partial P}{\partial z}$ = 1 MPa/mm	$\frac{\partial P}{\partial z}$ =2 MPa/mm	$\frac{\partial P}{\partial z}$ = 3MPa/mm
0.35	-0.4	0.00	0.00	0.00
0.45	-0.3	0.63	1.27	1.91
0.55	-0.2	1.02	2.06	3.09
0.65	-0.1	1.24	2.49	3.74
0.75	0	1.30	2.62	3.94
0.85	0.1	1.25	2.51	3.77
0.95	0.2	1.08	2.17	3.27
1.05	0.3	0.81	1.63	2.45
1.15	0.4	0.45	0.91	1.36
1.25	0.5	0.00	0.00	0.00

Now plotting the values of velocity for different radial position gives the following graph.

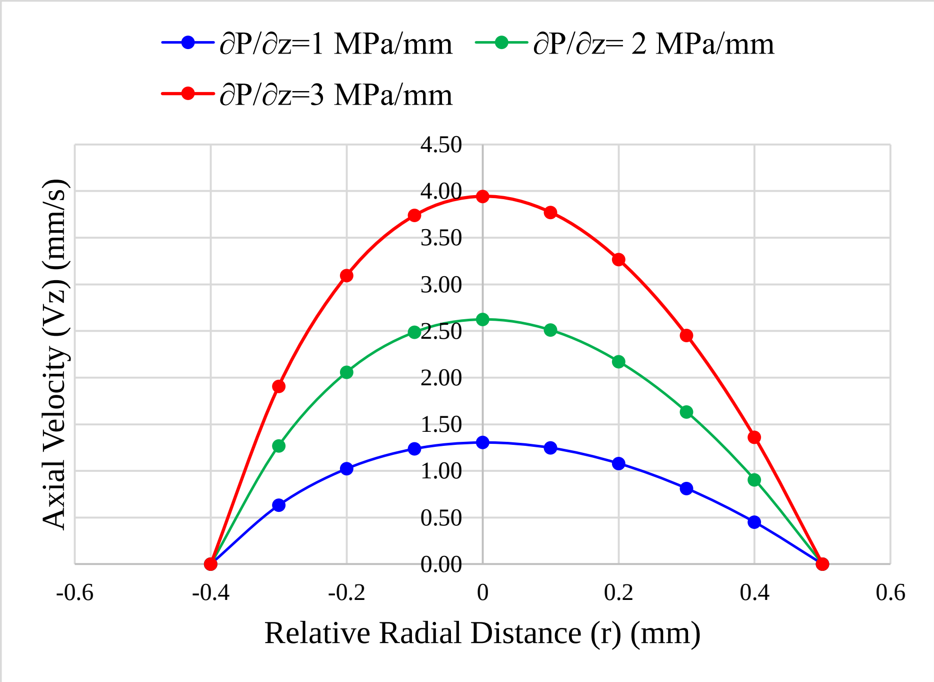

Figure 5.4. Velocity profile for different pressure gradient (Cylindrical Profile)

Now we will calculate the flow rate in this cylindrical region using the bellow derived formula for three different pressure.

$$Q = \frac{\pi(\,R_o^2 - R_i^2)}{8\mu}\left(-\frac{\partial P}{\partial \mathrm{z}} - \rho g\,\right)\left(R_o^2 + R_i^2 - \frac{\left(\,{R_o}^2 - {R_i}^2\right)}{\ln\left(\frac{R_o}{R_i}\right)}\right)$$

$\frac{\partial P}{\partial \mathrm{z}}$ (MPa/mm)	Q (mm^3/s)
3	11.70
2	7.79
1	3.87

In the following discussion, we analyze the flow behavior of molten plastic through a nozzle that transitions from a cylindrical to a conical section. The nozzle's design ensures that molten plastic flows around a central needle carrying nitrogen gas, creating an annular flow. In the cylindrical portion of the nozzle, both the inner and outer profiles are cylindrical. Here, the pressure and velocity are constant throughout the portion, leading to a uniform flow rate Q. In the conical portion, the inner profile remains cylindrical, while the outer profile is conical. The outer radius changes linearly from inlet (matching the outer diameter of the cylindrical portion) to a smaller outer radius at the outlet.

According to the continuity equation, the volumetric flow rate must remain constant throughout the nozzle. Thus, the flow rate at the inlet of the conical region (Q_1) is equal to the flow rate at the outlet (Q_2):

$$Q_1 = Q_2$$

This implies that the volumetric flow rate does not change along the conical section, but the pressure and velocity will vary due to the changing cross-sectional area. Now from the value of flow rate we will find out pressure gradient $\left(\frac{\partial P}{\partial z}\right)$ at the outlet and the using the velocity equation we will calculate the velocity at the exit point.

Q_2 (mm^3/s)	$\left(\frac{\partial P}{\partial z}\right)$ (Mpa/mm)	Outlet velocity (V_o) (mm/s)
11.70	50.31	10.18
7.79	33.48	6.77
3.87	10.4	3.37

Table 5.2 Velocity in the conical zone (nozzle orifice) for different calculated pressure gradient

r (relative)	r (mm)	V_z (mm/s)		
		$\left(\frac{\partial P}{\partial z}\right)$= 10.4 MPa/mm	$\left(\frac{\partial P}{\partial z}\right)$= 33.5 MPa/mm	$\left(\frac{\partial P}{\partial z}\right)$=50.3 MPa/mm
-0.2	0.35	0	0	0
-0.1	0.45	2.71	5.45	8.18
0	0.55	3.37	6.77	10.18
0.1	0.65	2.39	4.80	7.22
0.2	0.75	0	0	0

Now plotting the values of velocity for different radial position gives the following graph

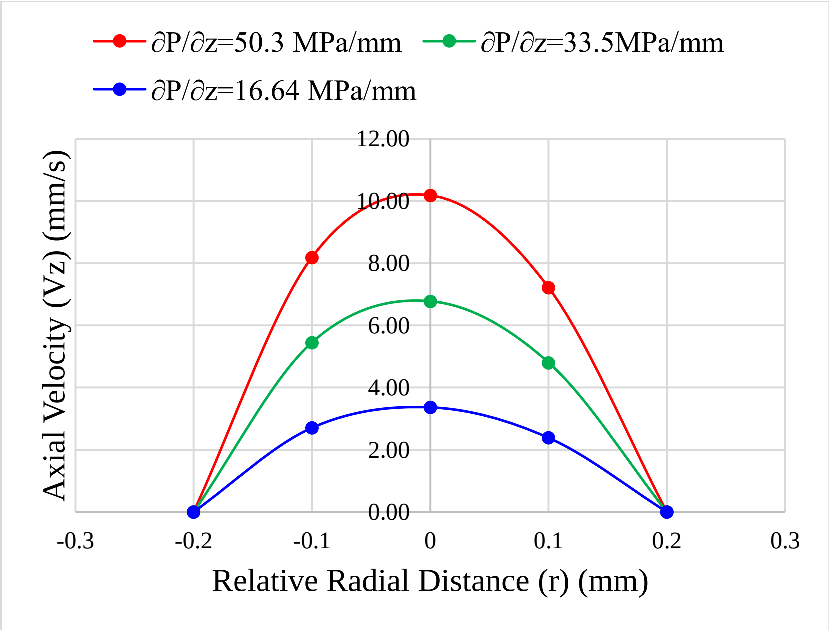

Figure 5.5. Velocity profile for different pressure gradient at nozzle orifice (Conical Profile)

In our experiment highest extrusion speed was around 10mm/s and lowest extrusion speed was 2.5mm/s, from here we can mark our work region in the conical portion.

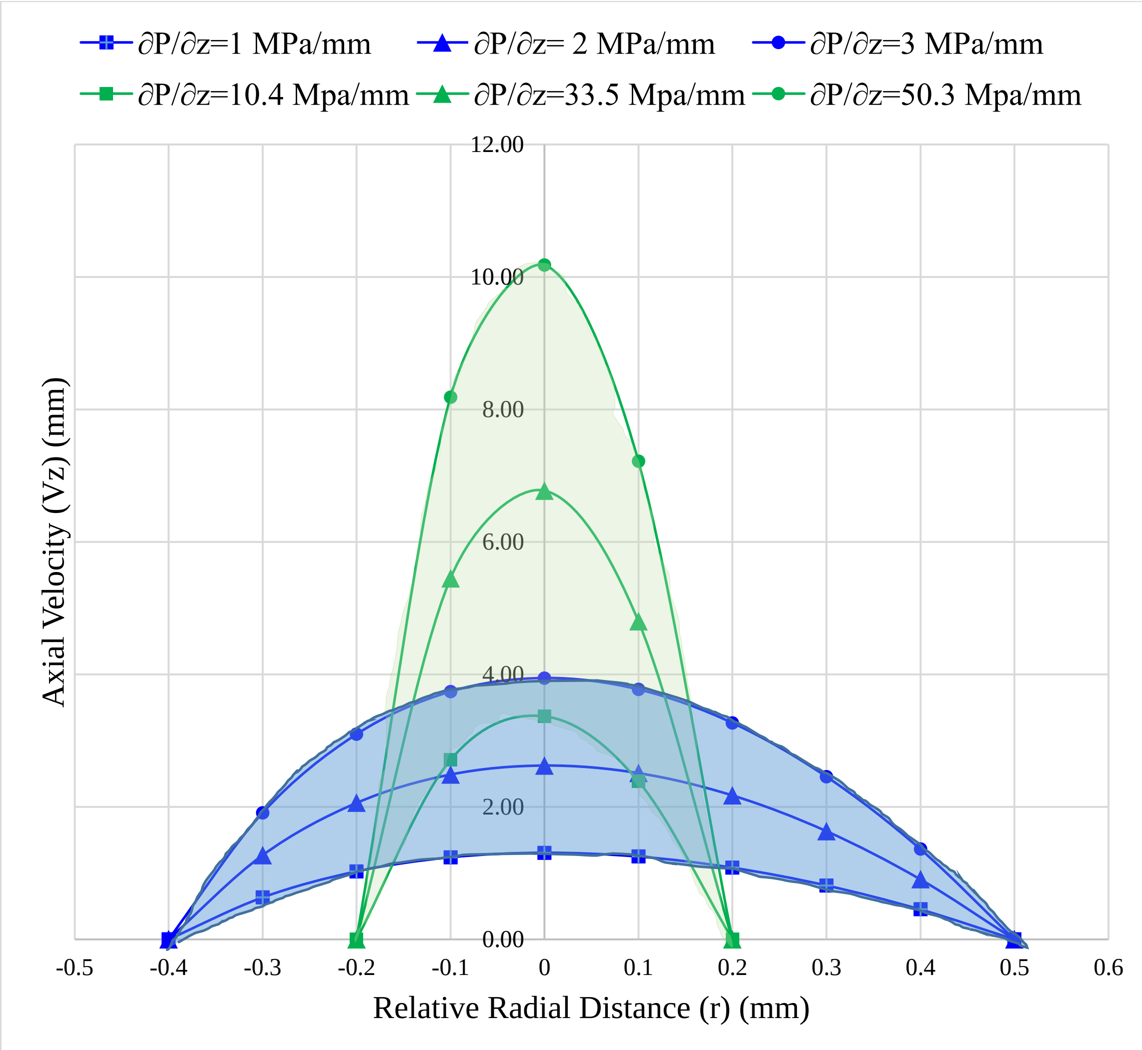

Figure 5.6 Velocity region in both cylindrical and conical portion of the nozzle

Chapter 6: Results and Discussion

6.1 Volumetric Flow Rate

The volumetric flow rate of a polymer in the context of additive manufacturing or extrusion processes refers to the volume of polymer material that flows through a specific section of the extrusion system per unit of time. Mathematically, the volumetric flow rate (Q) is defined as:

$$Q = \frac{V}{t}$$

where:

Q is the volumetric flow rate

V is the volume of the polymer passing through the extrusion system

t is the time over which the volume is measured (typically in seconds).

To calculate the volumetric flow rate, we initially allowed the PLA to extrude freely for a set duration, during which we measured both the mass and the flow time. From these measurements, we determined the mass flow rate. Using the following equation, we converted the mass flow rate to volumetric flow rate:

$$\rho = \frac{m}{V}, V = \frac{m}{\rho}$$

where:

ρ is the density of thermoplastic

m is the mass of the extrudate for a certain period of time

V is the volume of that extrudate

We gathered five samples for each combination of nozzle diameter, Gas pressure, and temperature, and then computed the average volumetric flow rate. Our experiment demonstrated that the volumetric flow rate of PLA increases with higher temperatures or Gas pressure.

The volumetric flow rate of a polymer generally increases with temperature due to enhanced mobility and decreased viscosity at higher temperatures. In rheology, the Vogel-Fulcher-Tammann (VFT) equation is often used to describe how viscosity depends on temperature in amorphous materials like glass-forming liquids or polymers [71,72]. The VFT equation is:

$$\eta = \eta_0 \, exp\left(\frac{B_{VFT}}{T - T_0}\right)$$

where:

η is the value of the viscosity at the temperature T,

η_0 is the value of the viscosity at the high temperature limit,

B_{VFT} is the activation energy for viscous flow,

T is the absolute temperature,

T_0 is the so called "Vogel temperature" which represents the temperature at which the viscosity would become infinite.

To understand how the VFT equation demonstrates that an increase in temperature (T) leads to a decrease in viscosity (η), we need to focus on the exponential term $\exp(B_{VFT}/(T-T_0))$. When the temperature rises, the denominator $(T-T_0)$ increases, making the exponent more negative. As a result, the exponential term approaches zero, indicating that higher temperatures cause the viscosity to decrease.

We observed for PLA the highest volumetric flow rate of 5.07 mm^3/s at 205°C. Beyond this flow rate, the extrusion motor did not function properly. However, at 220°C, the maximum flow rate reached 10.06 mm^3/s because the higher temperature reduced the viscosity of the PLA, allowing the extrusion motor to handle a higher flow rate during our experiment.

In our inflatable extrusion experiment for additive manufacturing, we found that increasing Gas pressure led to a higher flow rate of the extrudate. This can be explained by the fact that higher Gas pressure exerts greater force on the molten polymer, pushing it more efficiently through the nozzle. Additionally, increased pressure reduces the viscosity of the polymer by enhancing the shear thinning effect, allowing them to flow more easily. This improved mobility and reduced viscosity under higher pressure result in a higher melt flow index, facilitating a smoother and faster extrusion process.

6.2 Effect of Extrusion Parameters

We conducted our experiment at two different temperatures, 205°C and 220°C for PLA and 220°C and 230°C for SEBS. For each temperature, with a constant nozzle diameter, we varied the extrusion speed and gas pressure to determine the maximum and minimum values of the extrudates for each parameter (extrusion speed and gas pressure). For each combination of temperature, extrusion speed, and gas pressure, we produced five sets of samples. Tiny cross-sections from each sample were observed microscopically to measure their average outer diameter, core diameter, and shell thickness. Table 3 and Table 4 records data for PLA and SEBS respectively for different process conditions.

Table 6.1. Data Collection for different Extrusion Parameters (PLA)

Nozzle Diameter	Extrusion Speed (mm/s)	Gas Pressure (KPa)	Average Mass (g)	Average Time (s)	Average Volumetric Flowrate (mm^3/s)	Average Outer Diameter (D) (mm)	Average Core Diameter (d) (mm)	Average Shell Thickness (t) (mm)
Temperature 220°C, PLA Density 0.00118 g/mm^3								
1.5	0.5	13.8	0.21±0.006	100.52±0.11	1.74±0.05	1.36±0.05	0.72±0.06	0.32±0.055
		17.2	0.21±0.01	100.63±0.07	1.77±0.09	1.39±0.07	0.77±0.07	0.31±0.07
1.5	1.5	13.8	0.42±0.021	67.49±0.21	5.23±0.26	1.46±0.06	0.82±0.02	0.32±0.04
		24.1	0.44±0.023	67.44±0.12	5.57±0.3	1.64±0.08	1.02±0.02	0.31±0.05
1.5	2.5	13.8	0.38±0.006	40.32±0.26	7.92±0.17	1.55±0.07	0.85±0.04	0.35±0.055
		27.6	0.43±0.017	40.30±0.07	9.04±0.37	1.79±0.10	1.09±0.03	0.35±0.065
1.5	3	13.8	0.35±0.045	33.90±0.16	8.75±0.21	1.60±0.07	0.87±0.04	0.37±0.055
		27.6	0.4±0.01	33.68±0.13	10.06±0.24	1.95±0.02	1.23±0.02	0.36±0.02
Temperature 205°C, PLA Density 0.00118 g/mm^3								
1.5	0.5	13.8	0.21±0.015	100.52±0.13	1.74±0.13	1.35±0.06	0.68±0.03	0.33±0.045
		27.6	0.21±0.006	100.60±0.1	1.80±0.05	1.56±0.04	0.93±0.07	0.31±0.055
1.5	1.5	13.8	0.4±0.026	67.51±0.22	5.02±0.32	1.44±0.09	0.74±0.03	0.35±0.06
		27.6	0.4±0.012	67.45±0.10	5.07±0.15	1.59±0.07	0.93±0.04	0.33±0.055

Table 6.2. Data Collection for different Extrusion Parameters (SEBS)

Nozzle Diameter	Extrusion Temperature (C)	Extrusion Speed (mm/s)	Gas Pressure (KPa)	Average Outer Diameter (D) (mm)	Average Core Diameter (d) (mm)	Average Shell Thickness (t) (mm)
1.5	220	3	13.8	1.70	1.11	0.30
			20.7	1.75	1.16	0.30
1.5	220	6	13.8	1.76	1.13	0.31
			20.7	1.85	1.22	0.31
1.5	220	9	13.8	1.81	1.17	0.32
			20.7	1.99	1.37	0.31
1.5	230	3	13.8	1.74	1.20	0.27
			20.7			
1.5	230	6	13.8	1.80	1.23	0.28
			20.7	1.86	1.31	0.27
1.5	230	9	13.8	1.90	1.29	0.30
			20.7	2.05	1.50	0.28

6.2.1 Temperature Effect

The experiment showed that temperature significantly affects the dimensions of the extrudates. For PLA as the temperature increased from 205°C to 220°C, both the outer and inner diameters of the extrudates grew, while the shell thickness decreased. At 220°C, the highest outer and core diameters achieved were 1.95mm and 1.23mm, respectively while the extrusion speed was 3mm/s. At lower temperature, 205°C, highest achieved extrusion speed was 1.5mm/s and at that condition the outer and inner diameters were 1.59mm and 0.93mm, respectively. For a more accurate comparison, we examined the extrudates' dimensions at the same Extrusion speed. At 220°C, with an extrusion speed of 1.5mm/s, the outer and inner diameters were 1.64mm and 1.02mm. When we shifted the experiment from 205°C to 220°C while maintaining the same extrusion speed, the shell thickness of the extrudates decreased from 0.33mm to 0.31mm. At higher temperatures, the molten PLA can expand more easily under the influence of the nitrogen gas, resulting in larger diameters and thinner walls. The same characteristics were found for SEBS. With the increase of temperature from 220°C to 230°C both the outer diameter core diameter was increased and shell thickness decreased. We observed this relation for four different conditions and found the same result. This behavior suggests that temperature control is critical for achieving the desired dimensions and mechanical properties in the final extruded product. Figure 6.1, Figure 6.2, and Figure 6.3, shows how outer diameter (OD), core diameter (CD), and shell thickness (ST) changed with temperature for a certain extrusion speed and gas pressure for both PLA and SEBS.

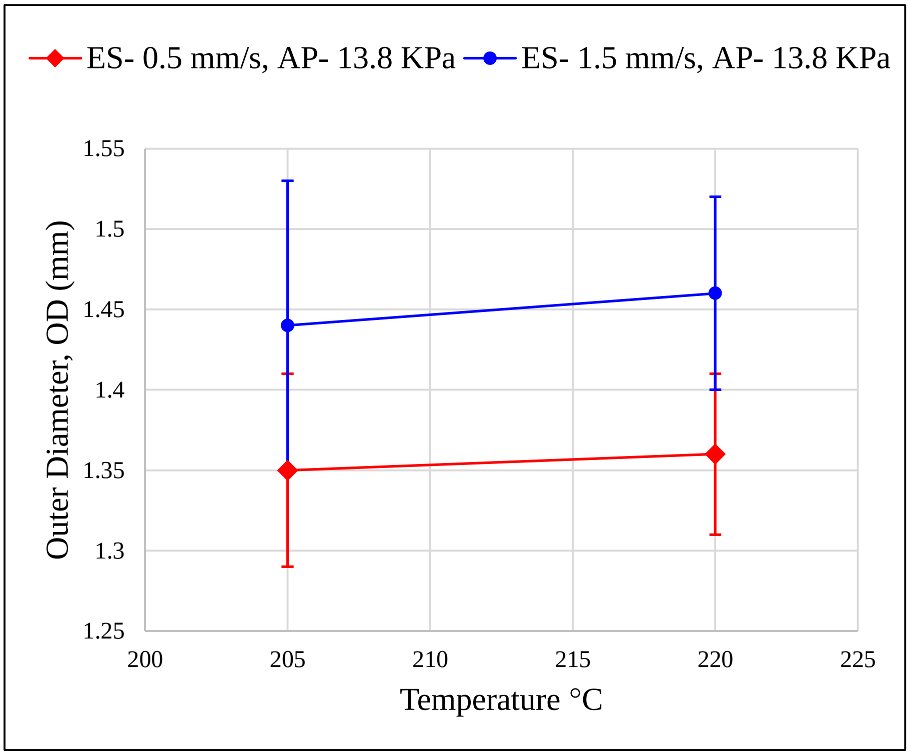

a)

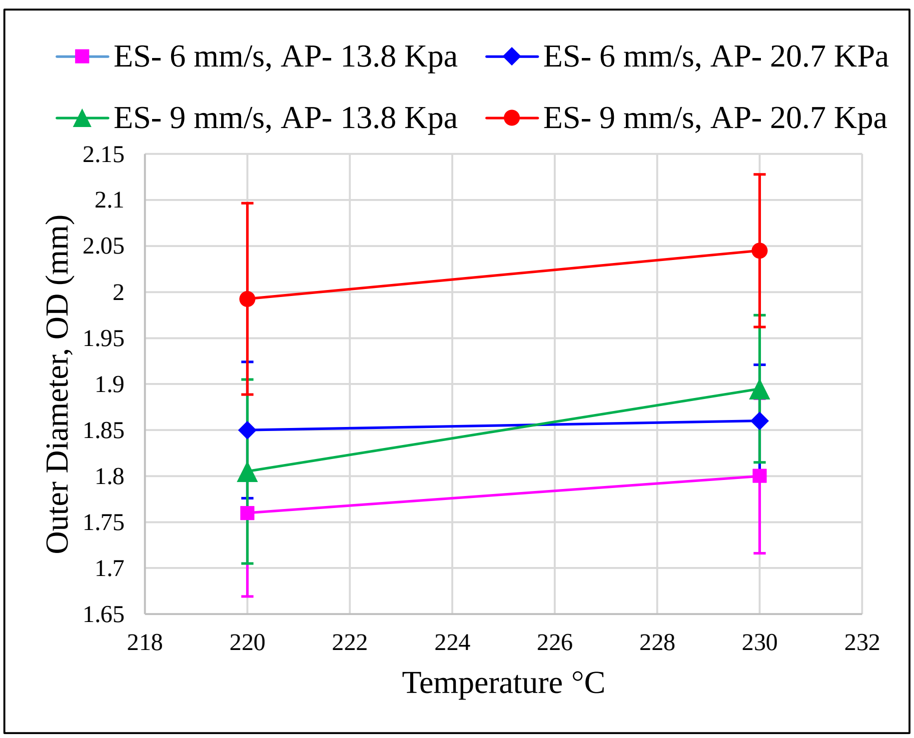

b)

Figure 6.1. Outer Diameter of Extrudates as a Function of Temperature a) PLA b) SEBS

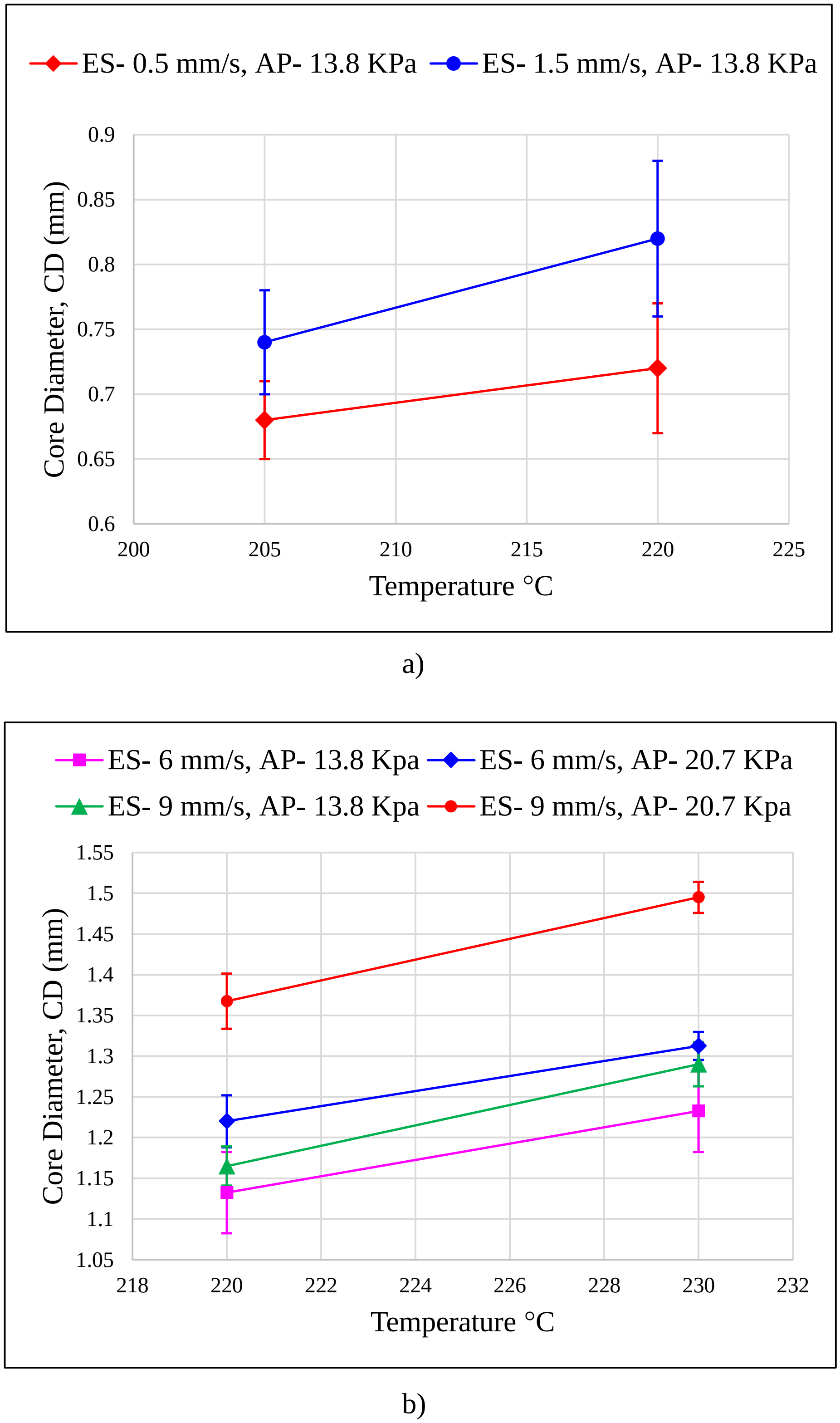

Figure 6.2. Core Diameter of Extrudates as a Function of Temperature, a) PLA, b) SEBS

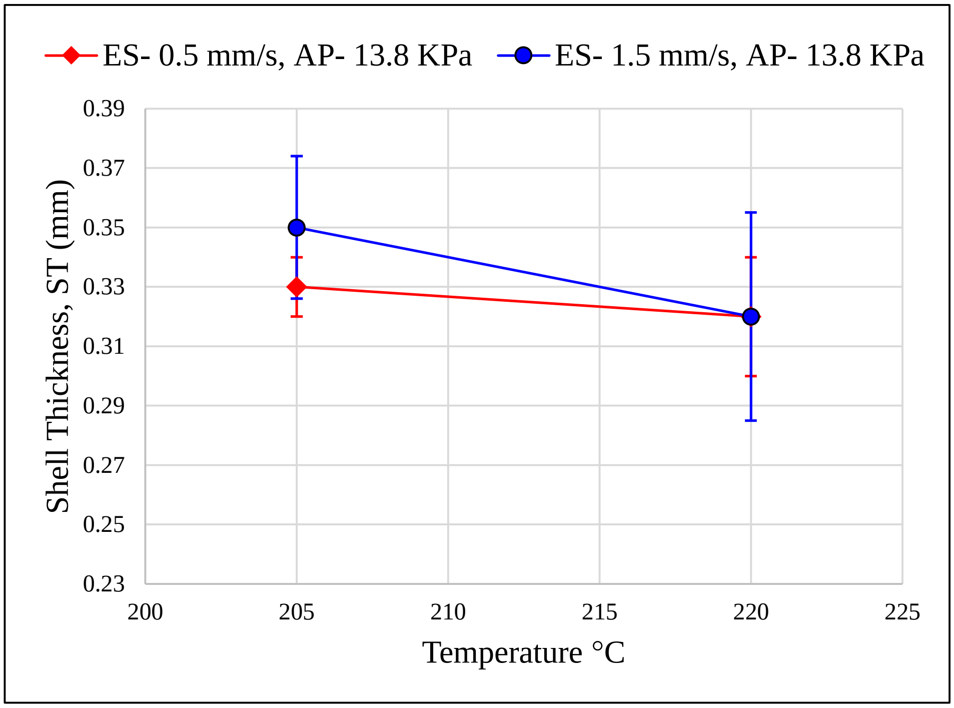

a)

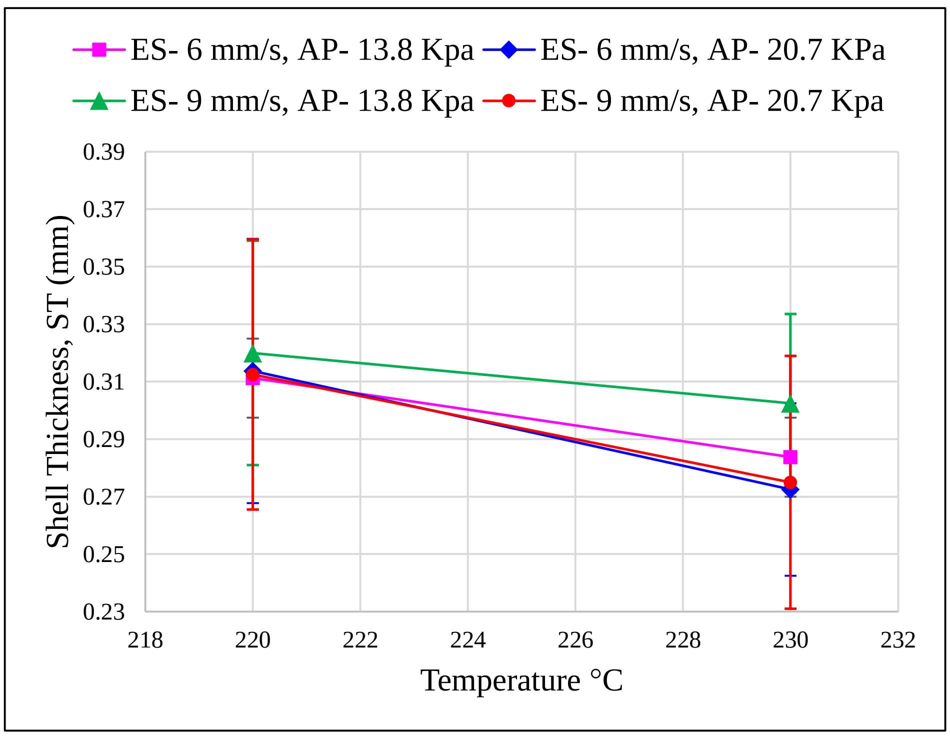

b)

Figure 6.3. Shell thickness of Extrudates as a Function of Temperature a) PLA, b) SEBS

6.2.2 Gas Pressure Effect

Gas pressure also played a crucial role in determining the dimensions of the extrudates. With a constant temperature and extrusion speed, an increase in gas pressure led to an increase in both the core and outer diameters of the extrudates, while the shell thickness decreased. Higher gas pressure forces more nitrogen gas into the molten PLA, causing greater expansion of the extrudate. This expansion increases the internal cavity size (core diameter) and the overall size (outer diameter) of the extrudate. However, as the material expands, the shell or wall of the extrudate becomes thinner due to the stretching effect caused by the higher internal pressure. These results indicate that controlling gas pressure is essential for managing the structural integrity and thickness of hollow extrudates in additive manufacturing processes.

The effect of gas pressure on SEBS is similar to PLA. For different process combinations with the increase of gas pressure from 13.8 KPa to 20.7 KPa both the outer diameter (OD) and core diameter (CD) increased, but shell thickness (ST) decreased.

Figure 6.4, Figure 6.5, and Figure 6.6 show the changes in outer diameter (OD), core diameter (CD), and shell thickness (ST) for both materials PLA and SEBS due to changes in gas pressure, while the other parameters were kept constant.

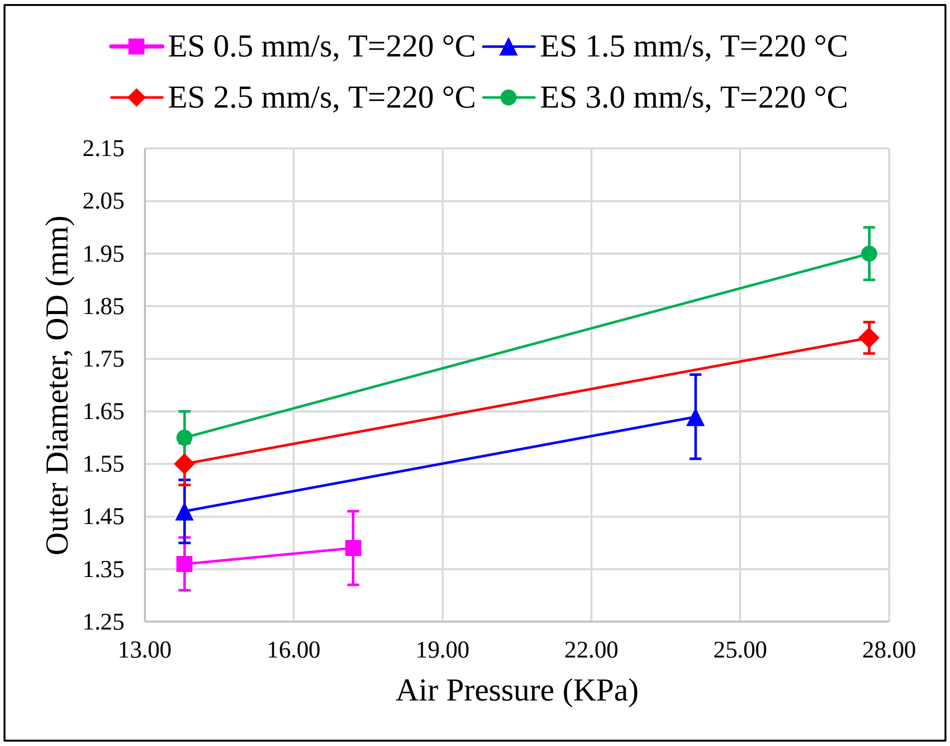

a)

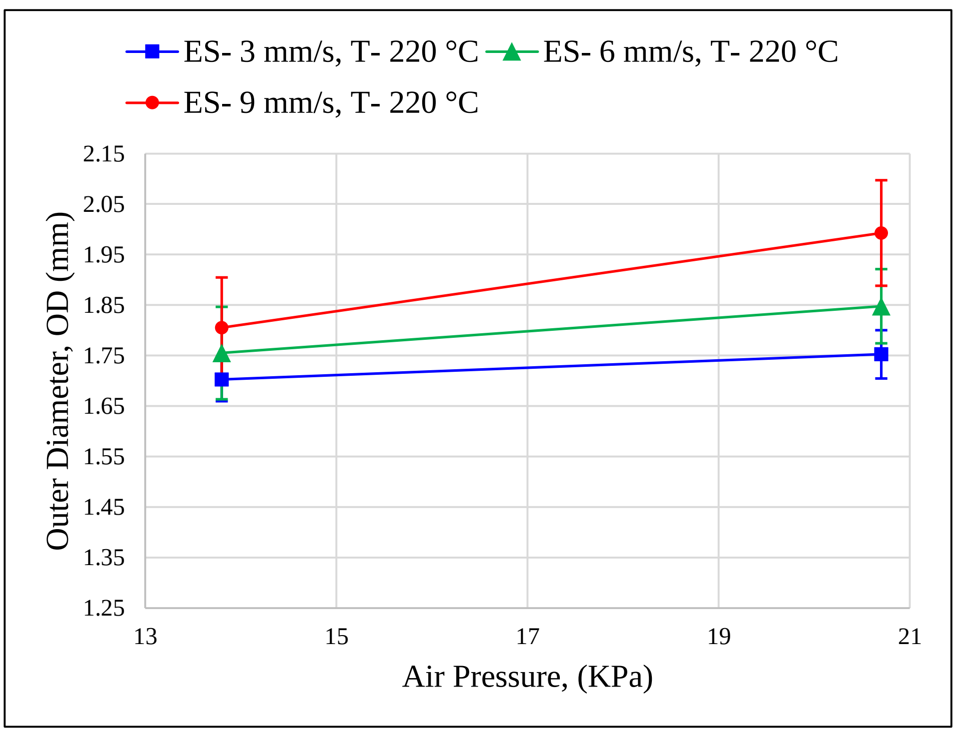

b)

Figure 6.4. Effect of Gas Pressure on Outer Diameter a) PLA b) SEBS

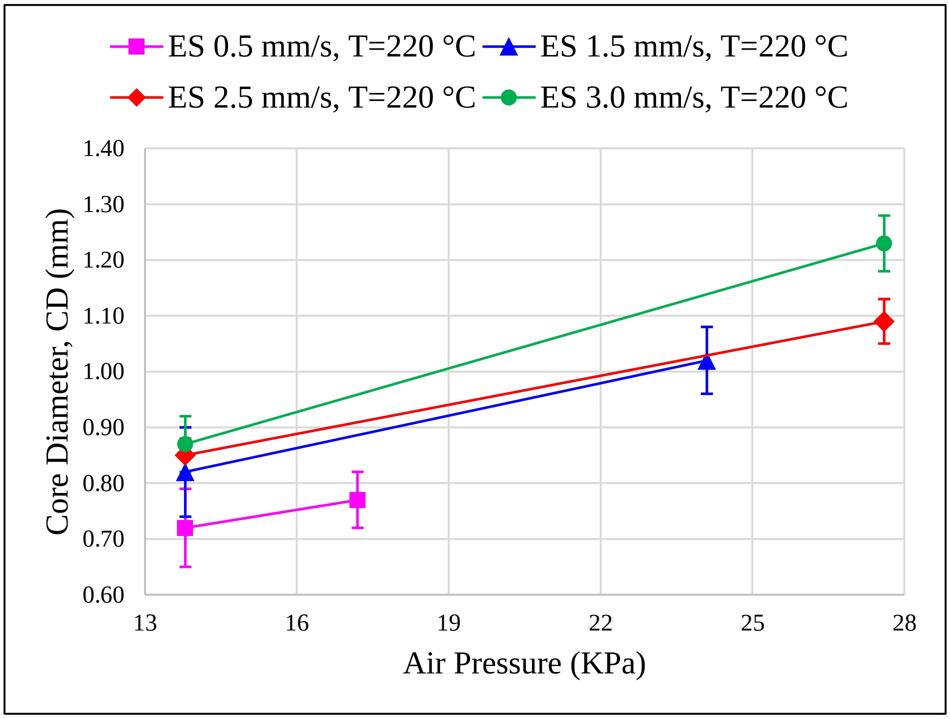

a)

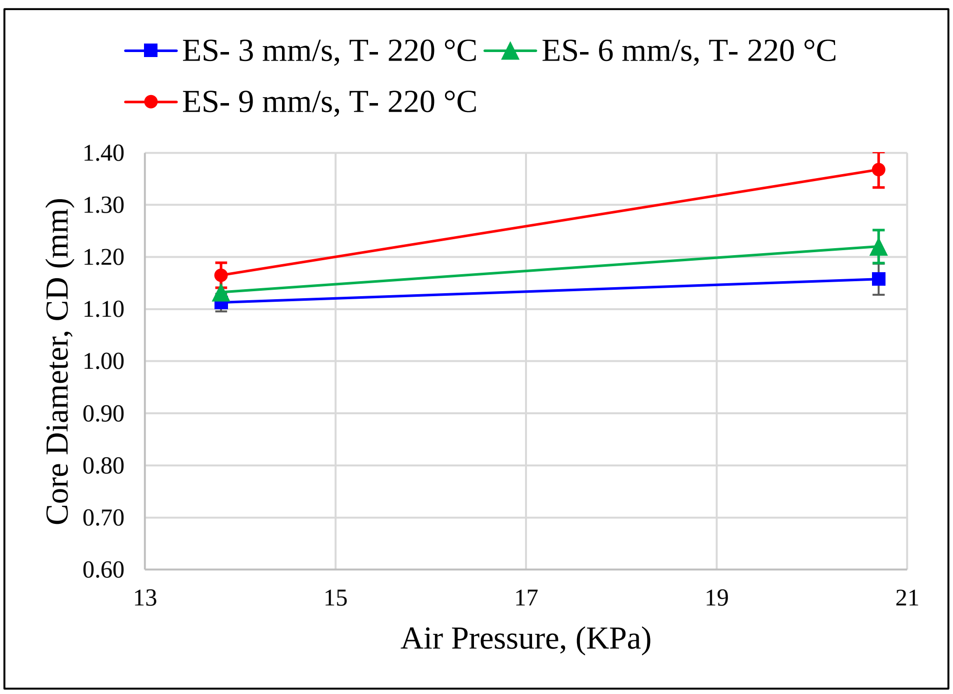

b)

Figure 6.5. Effect of Gas Pressure on Core Diameter a) PLA b) SEBS

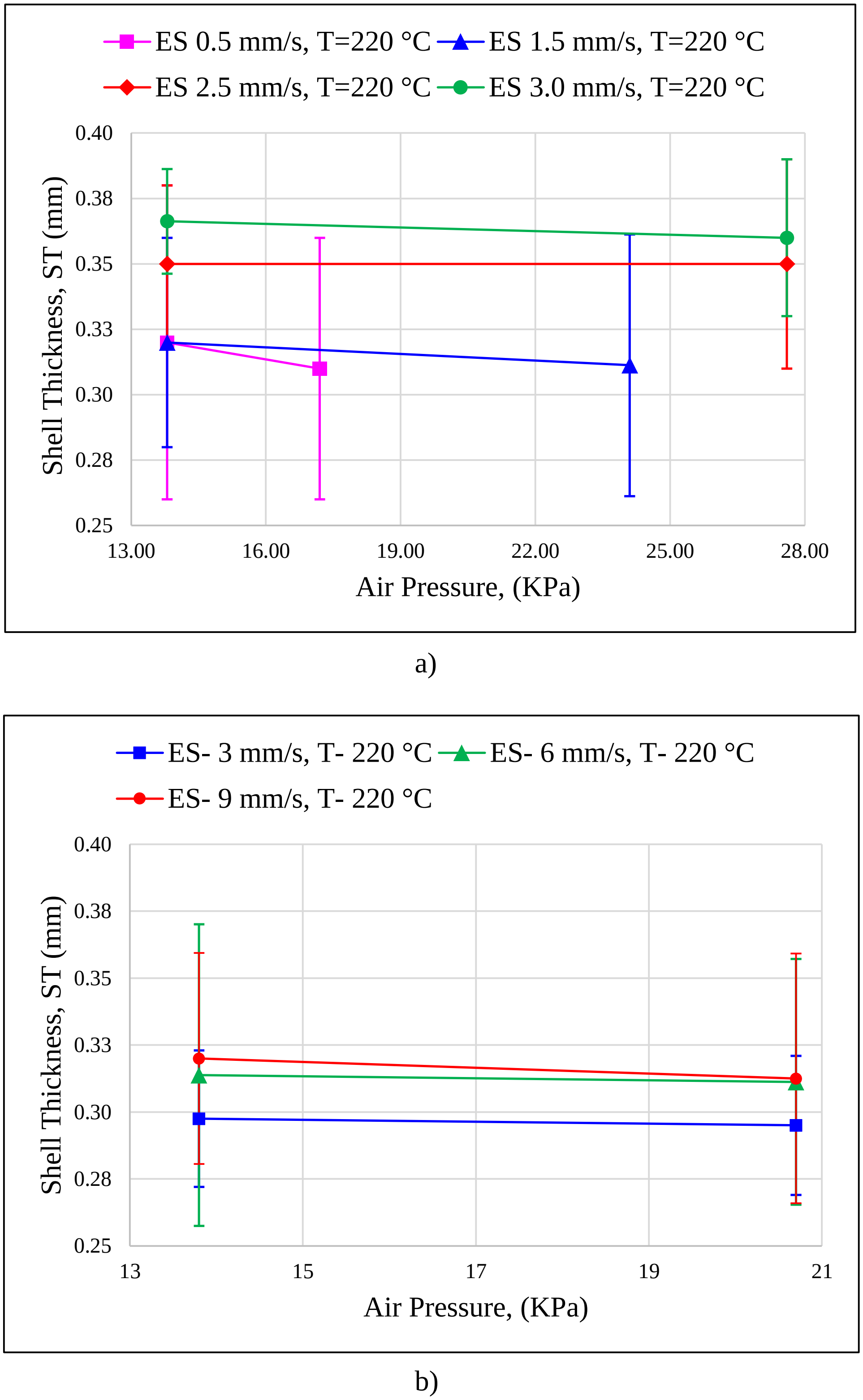

Figure 6.6. Effect of Gas Pressure on Shell Thickness a) PLA b) SEBS

6.2.3 Extrusion Speed Effect

The extrusion speed also had a significant impact on the extrudates' dimensions. With constant temperature and gas pressure, an increase in the extrusion speed led to increases in the outer diameter, core diameter, and shell thickness of the extrudates. By changing the extrusion speed we changed the volumetric flow rate. This can be explained by the greater volume of extruded material, allowing for more material to be expanded under the same conditions. The increased flow of material provides a larger mass to be shaped and expanded by the gas pressure, resulting in larger and thicker extrudates. Conversely, reducing the volumetric flow rate decreases the material available for expansion, leading to smaller outer and core diameters, and thinner extrudates. This highlights the importance of precise control over the flow rate to achieve consistent and desired outcomes in the extrusion process.

We got similar behavior from both materials PLA and SEBS. For both of these materials, we experimented with two different temperatures. For PLA we used temperatures 205°C and 220°C and in the case of SEBS we used temperatures 220°C and 230°C and in all conditions, both of these materials behaved similarly. Figure 6.7 and Figure 6.8 show the effect of extrusion speed on extrudates dimensions for PLA and SEBS respectively.

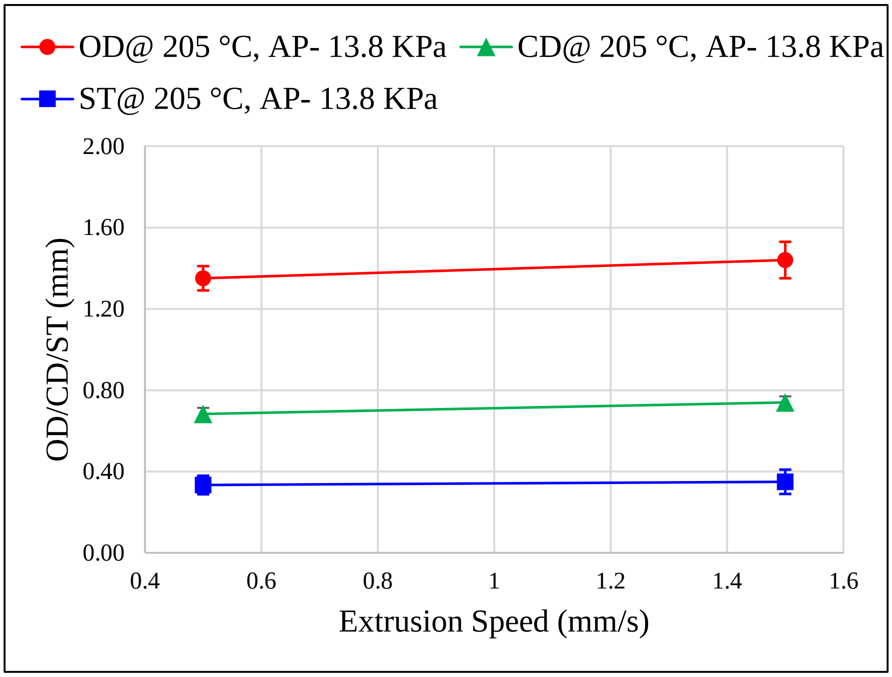

a)

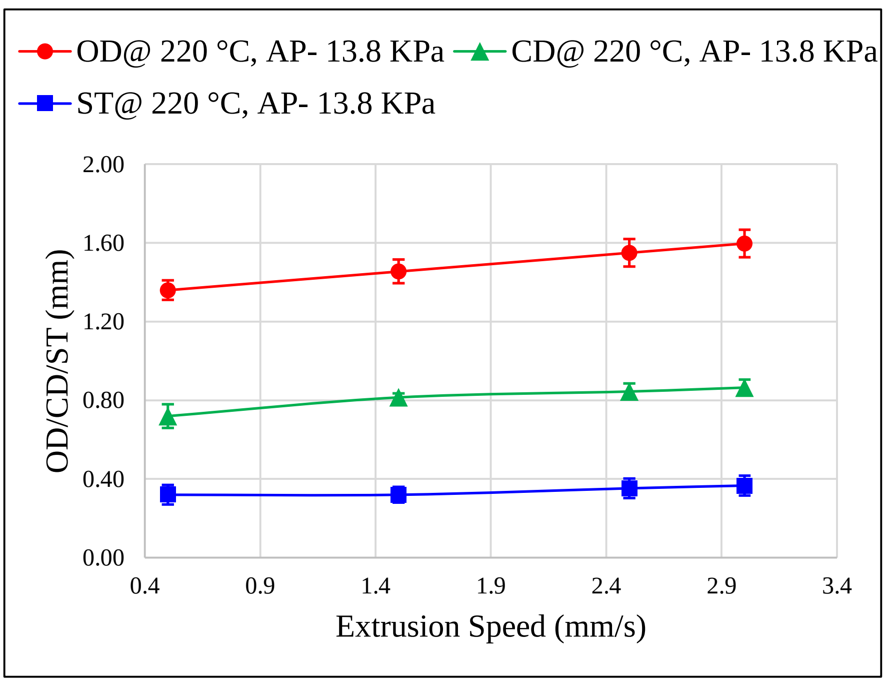

b)

Figure 6.7. Effect of Extrusion Speed over OD/ID/ST a) 205° C b) 220° C (Material: PLA)

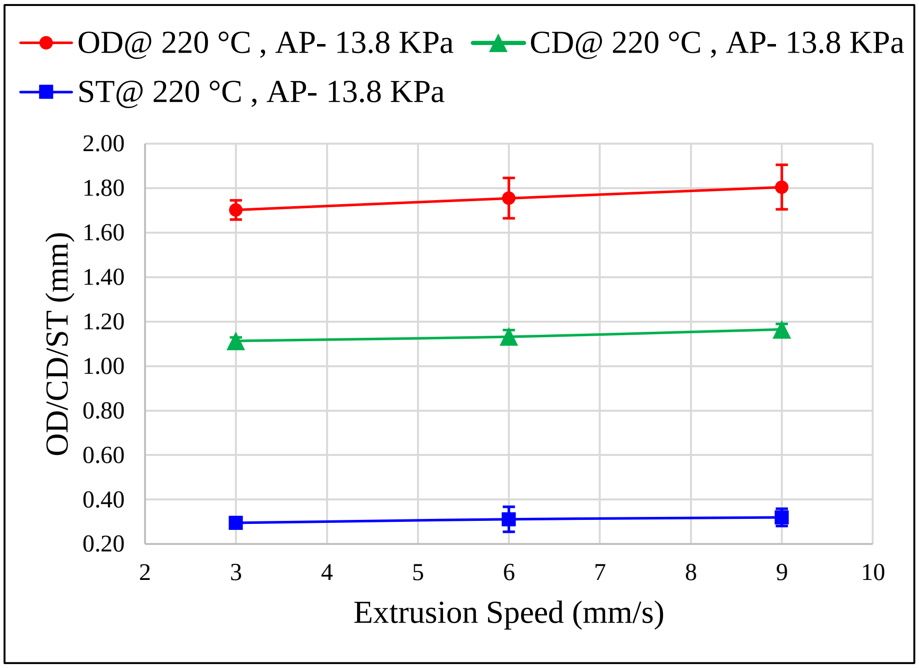

a)

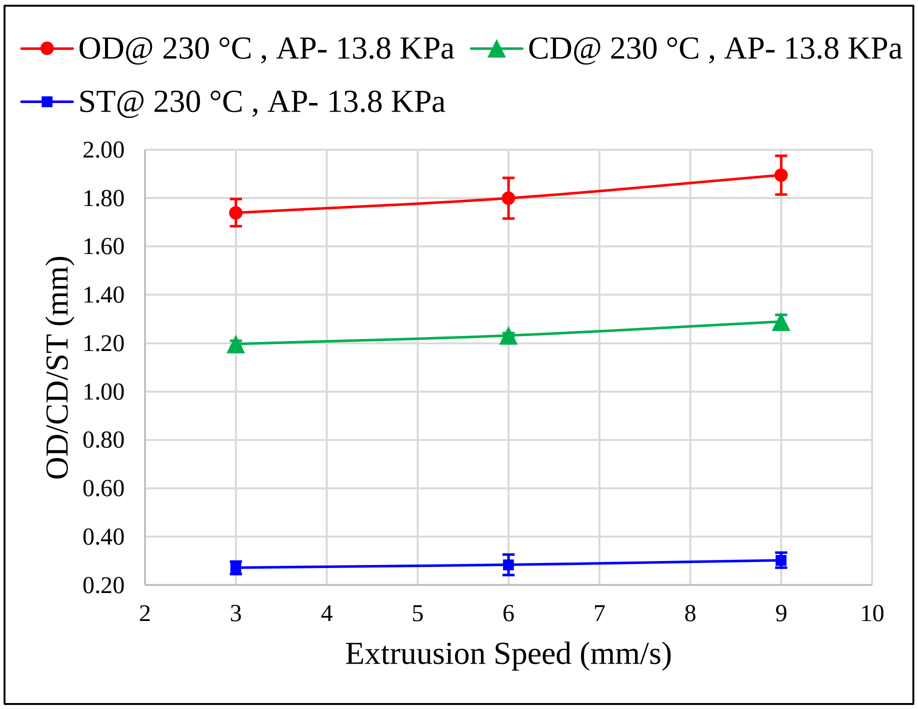

b)

Figure 6.8. Effect of Extrusion Speed over OD/CD/ST a) 220 °C b) 230 °C, Material: SEBS

6.3 Morphological Observation

We also captured microscopic images under various conditions, for both PLA and SEBS as illustrated below. In Figure 6.9 a), the notation '1.5_205_0.5_13.8' signifies that the sample was obtained using a 1.5 mm diameter nozzle, at a temperature of 205°C, with an extrusion speed of 0.5mm/s, and a gas pressure of 13.8 KPa. For material PLA we collected samples for twelve different process combinations and for SEBS we observed samples for 11 different combinations shown in figure 6.10.

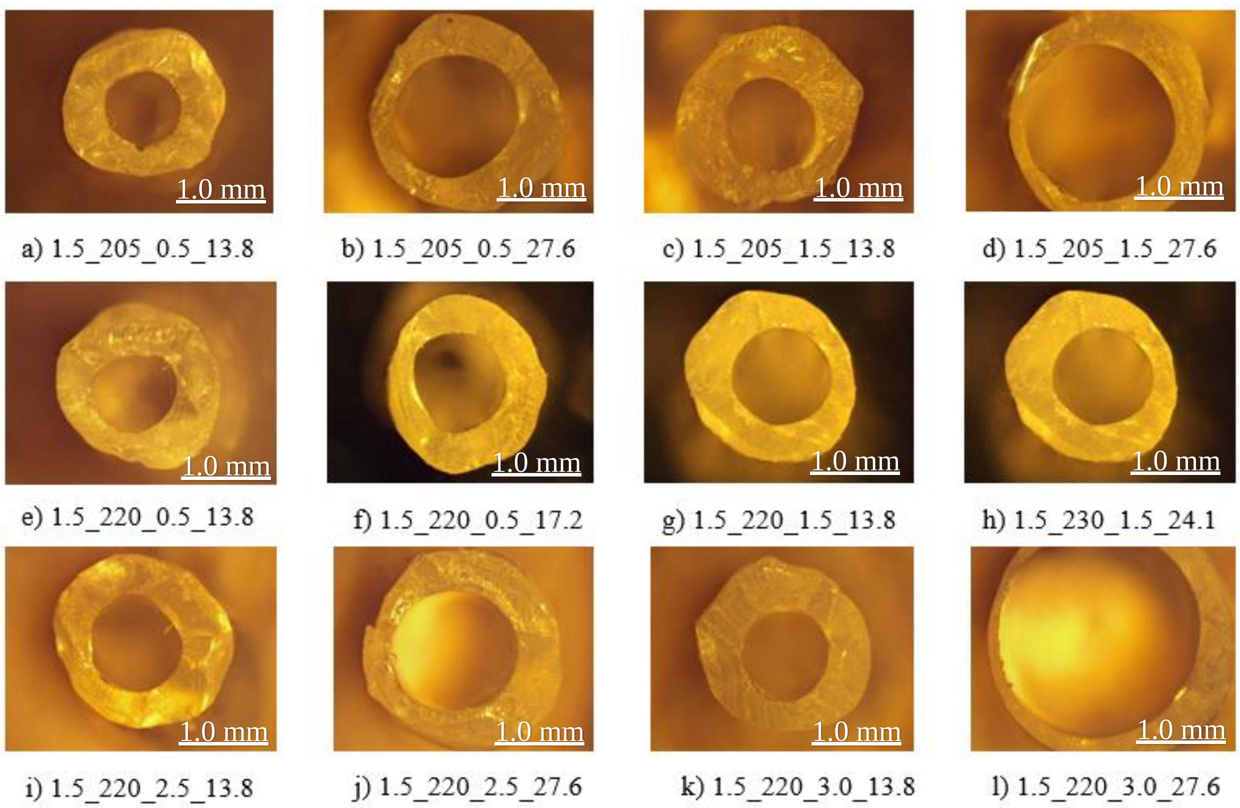

Figure 6.9. Microscopic images of extrudate cross sections for different extrusion conditions. Material: PLA

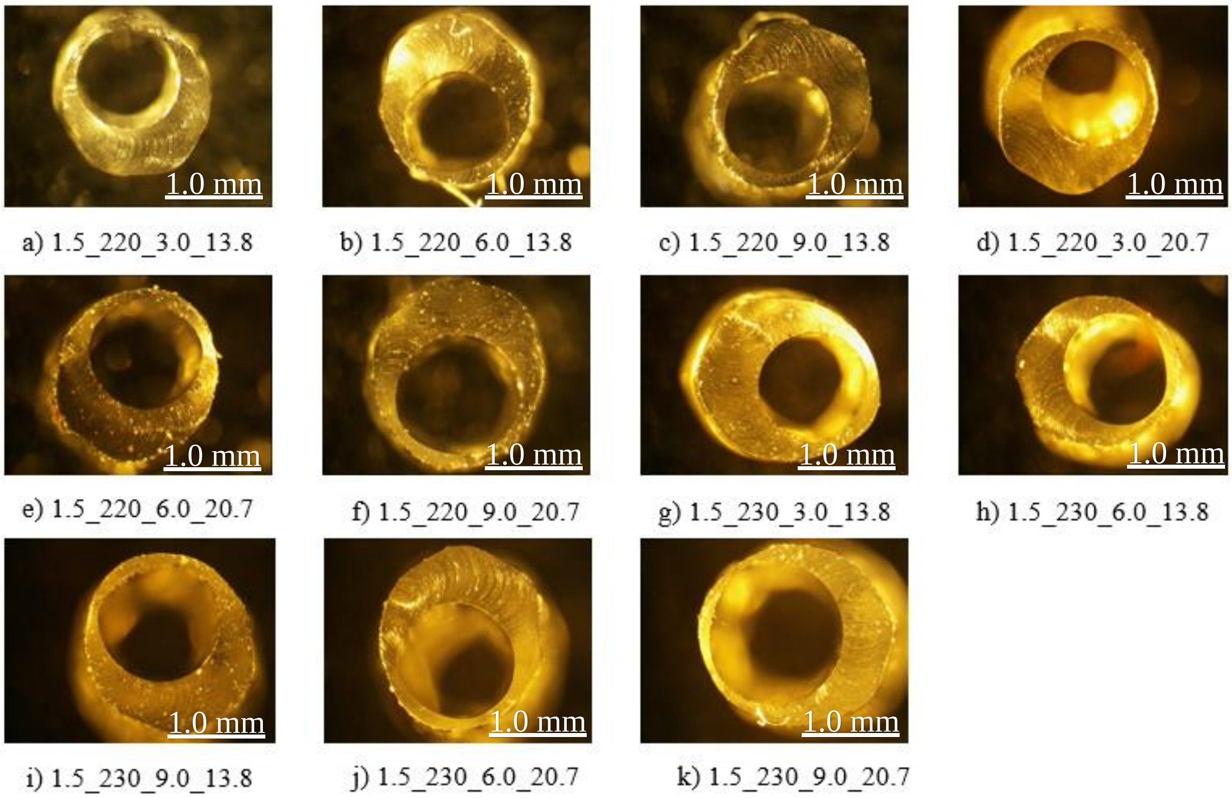

Figure 6.10. Microscopic images of extrudate cross sections for different extrusion conditions. Material: SEBS

Chapter 7: Conclusion

7.1 Conclusion

Since the invention of additive manufacturing in the late 1980s, the technology has made significant advancements but still faces challenges in creating objects with complex internal geometries and variable densities directly from printing. Current methods primarily focus on solid material extrusion, limiting the ability to produce items with internal voids or varied densities without extensive post-processing. This limitation poses a significant challenge for applications that require customized mechanical properties, lightweight yet strong structures, or objects needing varying material composition and structure.

To address this challenge, our primary objective is to establish a comprehensive methodology that enables the controlled inflation of thermoplastic extrudates during the additive manufacturing process. This involves determining the optimal conditions under which thermoplastics can be extruded and inflated to achieve the desired shapes and structures. The methodology encompasses the selection of suitable materials, the design and calibration of the pellet extruder, and the precise control of process parameters such as temperature, pressure, and extrusion speed.

For our experiment, we selected two different materials: PLA, a thermoplastic, and SEBS, a thermoplastic elastomer. PLA's biodegradability and ease of processing, combined with SEBS's flexibility and durability, allowed us to thoroughly evaluate the versatility and effectiveness of our developed methodology across different types of thermoplastics and elastomers.

To create inflatable hollow extrudates, we developed a setup with several key components. Nitrogen gas, stored in a cylinder, was regulated by a gas pressure regulator and connected to a soft PVC tube. This tube delivered the gas to the nozzle orifice of the hex extruder, which was equipped with a dispensing needle. The hex extruder was connected to the pellet extruder, and the hot-end of the 3D printer was modified to accommodate this extruder. The temperature in the hex extruder was controlled by a heater connected to a temperature controller. This setup allowed us to achieve controlled extrusion of inflatable hollow extrudates, combining innovative design and advanced technology in additive manufacturing.

We used a 1.5mm orifice diameter nozzle and selected two different temperatures for both PLA and SEBS for the experiment. At each temperature, we varied the gas pressure and polymer flow rate and collected five samples for each process combination. Cross-section samples were taken from each specimen and observed under a microscope. Since the extruded samples were not completely circular, we measured the outer diameter and core diameter at different positions of the cross-section and averaged those values. Dividing the difference between the outer and core diameter by two gave us the shell thickness. Multiple microscopic images were taken for each sample, and the best one was included in this study.

This comprehensive approach allowed us to evaluate the controlled inflation of thermoplastic extrudates, providing valuable insights into the optimization of process parameters for achieving desired geometries and structures in additive manufacturing. We also developed an analytical model in two different portions of nozzle (cylindrical and conical). We observed how velocity changes with different pressure and how pressure and velocity changes in different position of the conical section while maintaining the same pressure in the cylindrical portion. All the observed results were plotted in graphs.

7.2 Challenges and Limitations

In the journey to develop an effective additive manufacturing process for inflatable thermoplastics, we encountered numerous challenges that highlighted the intricate balance required between temperature, gas pressure, and material flow. Accurate control over these parameters was crucial to ensure consistent quality and functionality of the printed parts. Despite our efforts, maintaining this control proved to be a significant hurdle.

Temperature control was one of the primary issues we faced. Utilizing a temperature controller to maintain a steady state, we observed that most of the time, the temperature remained stable. However, there were instances where the temperature fluctuated above and below the preset value. These fluctuations were detrimental, as they affected the viscosity of the thermoplastic and consequently the quality of the extrudate. Consistent temperature is vital to ensure uniform melt flow and proper inflation, and these variations led to inconsistencies in the printed samples.

Gas pressure control was another critical parameter that posed significant challenges. The inflation of the extrudate relied heavily on the precise regulation of gas pressure. Our digital gas pressure regulator, while generally effective, often sensed fluctuations, causing slight variations in the inflation process. These variations led to inconsistencies in the wall thickness and overall structure of the inflated parts. Achieving and maintaining a constant gas pressure is essential for uniformity, and our inability to do so consistently resulted in suboptimal samples.

The flow rate of the material was also inconsistent throughout our experiments. This inconsistency contributed to different masses for parts printed with the same process parameters. The Mahor extruder occasionally struggled to deliver a steady melt flow, which was evident during the vertical extrusion process and printing. The extruded samples exhibited twisting, curling, and movement, leading to an eccentric inner hollow circle relative to the outer diameter. Controlling this twisting or curling motion was a challenge we were unable to overcome, affecting the precision and quality of the final product.

Manual adjustment of nitrogen gas pressure was required to control inflation for samples with varying densities in different sections. This manual intervention often resulted in inconsistent samples, highlighting the need for an automated and precise control mechanism. Additionally, nozzle clogging became a recurrent issue. This normal phenomenon, over time, caused variations in the printed samples despite using the same process parameters. We did not monitor nozzle wear or needle eccentricity after several months of use, which likely exacerbated this issue, as we had only one nozzle available.

Finally, we developed an analytical model for the annular flow inside our nozzle. However, due to the inability to measure the pressure of the polymer melt within the nozzle, we had to assume the pressure values. Moreover, we could not find viscosity data as a function of shear rate and temperature for PLA at the temperatures used in our experiments. Consequently, we had to assume viscosity values for our model, which introduced uncertainties in our analytical predictions.

In summary, the development of an inflatable additive manufacturing process for thermoplastics presented numerous technical challenges. Accurate control of temperature, gas pressure, and material flow was crucial but difficult to achieve consistently. The variability in materials, the need for precise control mechanisms, and the limitations of our experimental setup highlighted the complexity of this innovative manufacturing approach. Despite these challenges, the insights gained from our experiments provided valuable lessons for future improvements and optimizations in the process.

7.3 Future Recommendation

The primary objective of our experiment was to develop a methodology for creating inflatable extrudates using a pellet extruder, determining the process parameters, and understanding their interrelations for different materials. We successfully accomplished this goal, laying a strong foundation for future research and development in this field. However, this is just the beginning. There are numerous opportunities for further exploration and refinement, which can significantly enhance the accuracy, efficiency, and applicability of this technology.

One of the most critical areas for future improvement is enhancing process accuracy. The current setup, while effective, can be further refined with more precise equipment. Upgrading to a better pressure regulator will ensure more consistent inflation, reducing variability in the extrudates. Similarly, investing in a more accurate extruder and temperature controller will bring greater stability to the system, allowing for finer control over the extrusion process. These improvements will lead to more consistent results, ultimately enhancing the quality of the inflatable extrudates.

In addition to improving equipment, future research should focus on conducting comprehensive tests on the inflated extruded filament. While we have successfully created these extrudates, we have yet to perform essential tests such as tensile, impact, elasticity, flexibility, and flexural tests. Understanding the mechanical properties of the hollow extrudates is crucial for assessing their performance and potential applications. Moreover, it is well-known that hollow materials possess superior heat and sound insulation properties compared to solid materials. Conducting comparative tests on these properties will provide valuable insights into the benefits of hollow extrudates and help identify suitable applications.

Another important area for future research is the adhesion and layer bonding of the extrudates. Ensuring strong adhesion between layers is essential for maintaining the structural integrity of the printed objects. By experimenting with different materials and process parameters, we can optimize the layer bonding and enhance the overall durability of the extrudates. Additionally, using a larger diameter nozzle and a higher capacity extruder will allow us to explore a broader range of process parameters. This will enable us to better understand the system and identify optimal settings for different materials and applications.

Finding real-life applications for the hollow extrudates is another promising direction for future research. The unique properties of these extrudates, such as their lightweight and insulation capabilities, make them suitable for various industries, including aerospace, automotive, and construction. Conducting performance trials in real-world scenarios will help demonstrate the practical benefits of this technology and identify potential areas for commercial adoption. By collaborating with industry partners, we can further refine the process and develop customized solutions that meet specific industry needs.

While our research has successfully developed a methodology for creating inflatable extrudates using a pellet extruder, there is significant potential for further advancements. Enhancing process accuracy, conducting comprehensive mechanical tests, optimizing adhesion and layer bonding, and exploring real-life applications are critical areas for future research. By addressing these areas, we can unlock the full potential of this innovative technology, leading to more efficient, sustainable, and high-performance manufacturing solutions. This research represents the first step in a promising journey, and we are confident that it will inspire many more ideas and developments in the field of additive manufacturing.

References

1. Gao, W., Zhang, Y., Ramanujan, D., Ramani, K., Chen, Y., Williams, C. B., ... & Zavattieri, P. D. (2015). The status, challenges, and future of additive manufacturing in engineering. *Computer-Aided Design*, 69, 65-89.

2. Gibson, I., Rosen, D. W., & Stucker, B. (2010). *Additive manufacturing technologies* (Vol. 238). New York: Springer.

3. Ngo, T. D., Kashani, A., Imbalzano, G., Nguyen, K. T. Q., & Hui, D. (2018). Additive manufacturing (3D printing): A review of materials, methods, applications, and challenges. *Composites Part B: Engineering*, 143, 172-196.

4. Spatial. (2023, February 27). What is additive manufacturing? (Types, materials, and what to know). Spatial Blog. https://blog.spatial.com/what-is-additive-manufacturing

5. ASME. (n.d.). Infographic: The history of 3D printing. ASME. https://www.asme.org/topics-resources/content/infographic-the-history-of-3d-printing

6. Duhduh, A., Noor, H., Kundu, A., & Coulter, J. (2019). Advanced additive manufacturing of functionally gradient multi-material polymer components with single extrusion head: Melt rheology analysis.

7. Murr, L. E., Gaytan, S. M., Medina, F., Lopez, H., Martinez, E., Machado, B. I., ... & Wicker, R. B. (2010). Next-generation biomedical implants using additive manufacturing of complex, cellular and functional mesh arrays. *Philosophical Transactions of the Royal Society A: Mathematical, Physical and Engineering Sciences*, 368(1917), 1999-2032.

8. Zhang, C., Chen, Y., & Chen, H. (2021). Industry 4.0 and its Implementation: A Review. *Information Systems Frontiers*. https://doi.org/10.1007/s10796-021-10153-5

9. Lu, Y., & Ramakrishnan, S. (2019). The Direction of Industry: A Literature Review on Industry 4.0. *Proceedings of the International Conference on Engineering Design*, 1, 2191–2200.

10. Lasi, H., Fettke, P., Kemper, H.-G., Feld, T., & Hoffmann, M. (2014). Industry 4.0. *Business & Information Systems Engineering*, *6*(4), 239-242. https://doi.org/10.1007/s12599-014-0334-4

11. Qin, J., Liu, Y., & Grosvenor, R. (2016). A Categorical Framework of Manufacturing for Industry 4.0 and Beyond. *Procedia CIRP*, *52*, 173-178. https://doi.org/10.1016/j.procir.2016.08.005

12. Lu, Y. (2017). Industry 4.0: A Review on Industrial Automation and Robotic. *Journal of Industrial Integration and Management*, *2*(3), 1750016. https://doi.org/10.1142/S2424862217500162

13. Ford, S., & Despeisse, M. (2016). Additive manufacturing and sustainability: An exploratory study of the advantages and challenges. *Journal of Cleaner Production*, *137*, 1573-1587. https://doi.org/10.1016/j.jclepro.2016.04.150

14. Gao, W., Zhang, Y., Ramanujan, D., Ramani, K., Chen, Y., Williams, C. B., & Zavattieri, P. D. (2015). The status, challenges, and future of additive manufacturing in engineering. *Computer-Aided Design*, *69*, 65-89. https://doi.org/10.1016/j.cad.2015.04.001

15. Holmström, J., Liotta, G., & Chaudhuri, A. (2017). Sustainability outcomes through direct digital manufacturing-based operational practices: A design theory approach. *Journal of Cleaner Production*, *167*, 412-424. https://doi.org/10.1016/j.jclepro.2017.08.188

16. Berman, B. (2012). 3-D printing: The new industrial revolution. *Business Horizons*, *55*(2), 155-162. https://doi.org/10.1016/j.bushor.2011.11.003

17. Lipson, H., & Kurman, M. (2013). *Fabricated: The new world of 3D printing*. John Wiley & Sons.

18. Kodama, H. (1981). Rapid-prototyping system by using photopolymer and UV light. *Proceedings of the IET International Conference on Information Technology and Applications*, 207-210. https://doi.org/10.1049/cp:19810112

19. Hull, C. W. (1986). Apparatus for production of three-dimensional objects by stereolithography. U.S. Patent No. 4,575,330.

20. Texas Instruments. (1987). Digital Light Processing. Retrieved from https://www.ti.com/dlp-chip/overview.html

21. Deckard, C. (1988). Method and apparatus for producing parts by selective sintering. U.S. Patent No. 4,863,538.

22. ASME. (n.d.). Infographic: The history of 3D printing. Retrieved from https://www.asme.org/topics-resources/content/infographic-the-history-of-3d-printing

23. Crump, S. S. (1992). Apparatus and method for creating three-dimensional objects. U.S. Patent No. 5,121,329.

24. Helisys Inc. (1991). Laminated Object Manufacturing. Retrieved from https://www.laminatedobjectmanufacturing.com

25. Arcam AB. (1997). Electron Beam Melting (EBM). Retrieved from https://www.ge.com/additive/additive-manufacturing/machines/arcam-ebm

26. Sachs, E., Cima, M., Williams, P., Brancazio, D., & Cornie, J. (1992). Three-dimensional printing: Rapid tooling and prototypes directly from a CAD model. *Journal of Engineering for Industry*, *114*(4), 481-488. https://doi.org/10.1115/1.2900705

27. Pereira, T., Kennedy, J. V., & Potgieter, J. (2005). A comparison of traditional manufacturing vs additive manufacturing, the best method for the job. *Procedia Manufacturing*, *3*, 315-323. https://doi.org/10.1016/j.promfg.2015.07.124

28. Wohlers Associates. (2020). *Wohlers Report 2020: 3D Printing and Additive Manufacturing State of the Industry*. Fort Collins, CO: Wohlers Associates.

29. Murphy, S. V., & Atala, A. (2014). 3D bioprinting of tissues and organs. *Nature Biotechnology*, *32(8)*, 773-785. https://doi.org/10.1038/nbt.2958

30. Prakash, K. M., Sushil, R., & Singh, R. K. (2021). Additive manufacturing: Current scenario in automotive sector. *Materials Today: Proceedings*, *44*, 2460-2468. https://doi.org/10.1016/j.matpr.2020.12.715

31. Tumbleston, J. R., Shirvanyants, D., Ermoshkin, N., Janusziewicz, R., Johnson, A. R., Kelly, D., ... & DeSimone, J. M. (2015). Continuous liquid interface production of 3D objects. *Science*, *347(6228)*, 1349-1352. https://doi.org/10.1126/science.aaa2397

32. ASTM F42. (2021). Committee F42 on Additive Manufacturing Technologies. ASTM International. Retrieved from https://www.astm.org/COMMITTEE/F42.htm.

33. Gebhardt, A. (2012). *Understanding Additive Manufacturing: Rapid Prototyping, Rapid Tooling, Rapid Manufacturing.* Hanser Publishers.

34. Barnatt, C. (2016). *3D Printing: Third Edition*. CreateSpace Independent Publishing Platform.

35. Gibson, I., Rosen, D. W., & Stucker, B. (2015). *Additive Manufacturing Technologies: 3D Printing, Rapid Prototyping, and Direct Digital Manufacturing*. Springer.

36. Pereira, T., Kennedy, J. V., & Potgieter, J. (2015). A comparison of traditional manufacturing vs additive manufacturing, the best method for the job. *Procedia Manufacturing*, *3*, 315-323. https://doi.org/10.1016/j.promfg.2015.07.124

37. Turner, B. N., Gold, S. A., & Pearce, J. M. (2015). Anisotropic mechanical properties of fused deposition modeling 3D printed objects. *Additive Manufacturing*, *6,* 1-11. https://doi.org/10.1016/j.addma.2015.03.005

38. Pricci, A.; de Tullio, M.D.; Percoco, G. Analytical and Numerical Models of Thermoplastics: A Review Aimed to Pellet Extrusion-Based Additive Manufacturing. *Polymers* **2021**, *13*, 3160. https://doi.org/10.3390/polym13183160

39. Daminabo, S. C., Goel, S., Grammatikos, S. A., Nezhad, H. Y., & Thakur, V. K. (2022). Fused deposition modeling-based additive manufacturing (3D printing): Techniques for polymer material systems. *Materials Today Chemistry*, 25, 100564

40. Khosravani, M. R., & Reinicke, T. (2020). The impact of process parameters on the mechanical properties and dimensional accuracy of parts printed using pellet extrusion additive manufacturing. *Journal of Manufacturing Processes*, 48, 584-594.

41. Mohammed, M. I., Wilson, D., & Akindoyo, J. O. (2021). The application of pellet extrusion-based additive manufacturing for end-use products: A review. *Additive Manufacturing*, 37, 101647.

42. Bours, J., Chawla, K., & Mei, R. (2017). Investigation of pellet extrusion 3D printing for improved sustainability. *Journal of Cleaner Production*, 142, 3941-3951.

43. Liu, X., Zhang, Y., & Li, J. (2020). Long-term performance of pellet extrusion additive manufactured parts under various environmental conditions. *Materials Today Communications*, 25, 101466.

44. Hart, K., Rees, A., & Ding, J. (2022). Enhancing the mechanical strength of pellet extrusion additive manufactured parts through infill pattern optimization and thermal treatments. *Additive Manufacturing*, 40, 101921.

45. Gonzalez-Gutierrez, J., Arbeiter, F., Schlauf, T., Kukla, C., Felfer, P., & Pedersen, D. B. (2018). The effect of processing parameters on the mechanical properties of parts fabricated with an open-source pellet-extrusion additive manufacturing machine. *Additive Manufacturing*, 23, 99-108.

46. Hopkinson, N., & Dickens, P. M. (2003). Analysis of rapid manufacturing—using layer manufacturing processes for production. *Proceedings of the Institution of Mechanical Engineers, Part C: Journal of Mechanical Engineering Science*, 217(1), 31-39.

47. Peng, A., Wu, G., & Wang, Y. (2020). Investigation on why material properties of 3D printed parts are anisotropic based on the rheological behavior of the filament. *Additive Manufacturing*, 32, 101030.

48. Tirella, A., Vozzi, G., & Ahluwalia, A. (2014). Biomaterials and biofabrication for tissue engineering. *3D Printing and Additive Manufacturing*, 1(2), 87-95.

49. Tekinalp, H. L., Kunc, V., Velez-Garcia, G. M., Duty, C. E., Love, L. J., Naskar, A. K., Blue, C. A., & Ozcan, S. (2014). Highly oriented carbon fiber–polymer composites via additive manufacturing. *Composites Science and Technology*, 105, 144-150.

50. Zhong, Y., Godfrey, S., Jones, E., & Lilley, D. (2020). Recycling of thermoplastic composites for use in additive manufacturing. *Composites Part B: Engineering*, 187, 858.

51. Rodriguez, E. D., Vaidya, A., & Kunc, V. (2019). Large-scale additive manufacturing with bio-based thermoplastic feedstocks. *Journal of Manufacturing Processes*, 42, 47-54.

52. Coogan, T. J., & Kazmer, D. O. (2017). In-line rheological monitoring of fused deposition modeling. *Journal of Rheology*, 61(5), 1149-1157.

53. Liu, Z., Wang, Y., Wu, B., Cui, C., Guo, Y., Yan, C., & Shi, Y. (2019). A critical review of fused deposition modeling 3D printing technology in manufacturing polylactic acid parts. *International Journal of Advanced Manufacturing Technology*, 102(9), 2877-2889.

54. Thompson, M. K., Moroni, G., Vaneker, T., Fadel, G., Campbell, R. I., Gibson, I., ... & Martina, F. (2016). Design for additive manufacturing: Trends, opportunities, considerations, and constraints. *CIRP Annals*, 65(2), 737-760.

55. Wevolver. (n.d.). A comprehensive guide to PLA melting point and how it influences 3D printing. Wevolver. https://www.wevolver.com/article/a-comprehensive-guide-to-pla-melting-point-and-how-it-influences-3d-printing

56. 3D Systems. (n.d.). Introduction to the most common materials used for 3D printing. 3D Systems. https://www.3ds.com/make/solutions/blog/most-common-materials-3d-printing

57. Râpă, M., Darie-Nita, R., & Vasile, C. (2017). Influence of plasticizers over some physico-chemical properties of PLA. *Materiale Plastice, 54*(1), 73-78. https://doi.org/10.37358/MP.17.1.4789

58. Cubeddu, A., Fava, P., Pulvirenti, A., Haghighi, H., Saha, N., & Farris, S. (2021). Suitability assessment of PLA bottles for high-pressure processing of apple juice. *Foods, 10*(2), 295. https://www.mdpi.com/2304-8158/10/2/295

59. Kuraray. (n.d.). Styrene-Ethylene-Butylene-Styrene thermoplastic elastomer (SEBS). Kuraray Elastomer. Retrieved from https://www.elastomer.kuraray.com/us/blog/sebs/

60. Mahor XYZ. (n.d.). Homepage. Mahor XYZ. https://mahor.xyz/

61. Mahor XYZ. (n.d.). V4 pellet extruder [Product image]. Mahor XYZ. https://mahor.xyz/producto/v4-pellet-extruder/

62. Amazon.ca. (n.d.). Product page. Amazon. https://www.amazon.ca/dp/B01LY2IO6C?ref=cm_sw_r_cso_wa_apan_dp_4XVC93SZKQJW780EGTEZ&ref_=cm_sw_r_cso_wa_apan_dp_4XVC93SZKQJW780EGTEZ&social_share=cm_sw_r_cso_wa_apan_dp_4XVC93SZKQJW780EGTEZ&starsLeft=1

63. McMaster-Carr. (n.d.). https://www.mcmaster.com/1075T183/

64. McMaster-Carr. (n.d.). https://www.mcmaster.com/5233K121/

65. McMaster-Carr. (n.d.). https://www.mcmaster.com/51465K117/

66. McMaster-Carr. (n.d.). https://www.mcmaster.com/6710A29/

67. Creality. (n.d.). Ender-5 S1 3D printer. Creality Store. https://store.creality.com/ca/products/ender-5-s1-3d-printer?spm=..collection_f54d010d-3006-4cd2-bbe0-4803f859154.albums_1.1&spm_prev=..index.products_display_nav_1.1

68. Spool3D. (n.d.). Creality circuit board for Sprite extruder. Spool3D. https://spool3d.ca/creality-circuit-board-for-sprite-extruder/

69. Vallder. (n.d.). REX-C100 temperature controller. Vallder. https://vallder.com/product/rex-c100/

70. PRITCHARD, P. J., & LEYLEGIAN, J. C. (n.d.). Introduction to Fluid_Mechanics.

71. Darabi, L., & Zare, M. (2020). High correlate simple equations for temperature and pressure dependence of the viscosity of ionic liquids. Chemical Physics, 539. https://doi.org/10.1016/j.chemphys.2020.110933

72. Ikeda, M., & Aniya, M. (2013). Understanding the Vogel-Fulcher-Tammann law in terms of the bond strength-coordination number fluctuation model. Journal of Non-Crystalline Solids, 371–372, 53–57. https://doi.org/10.1016/j.jnoncrysol.2013.04.034

Appendices

Appendix A: Engineering Drawing

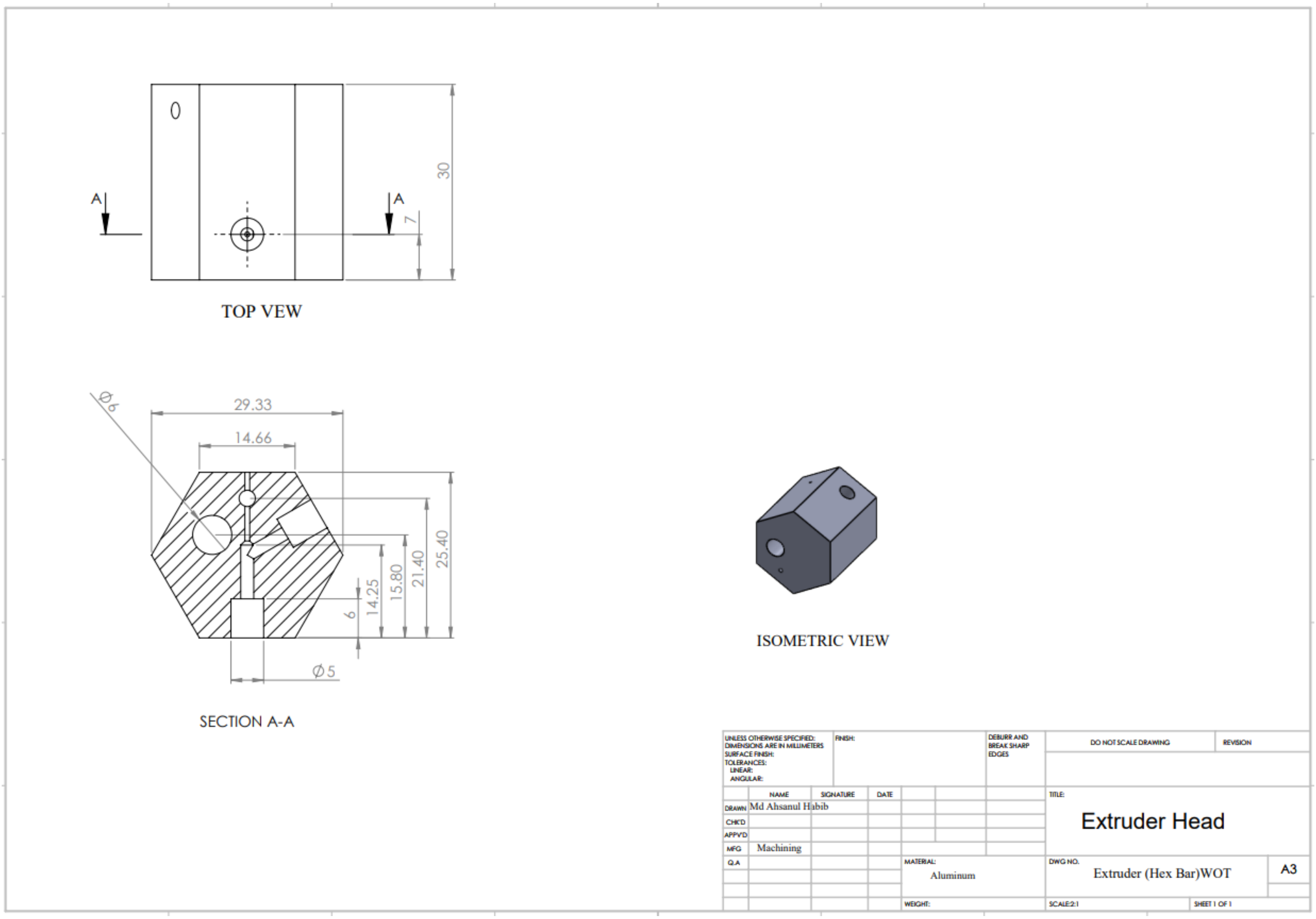

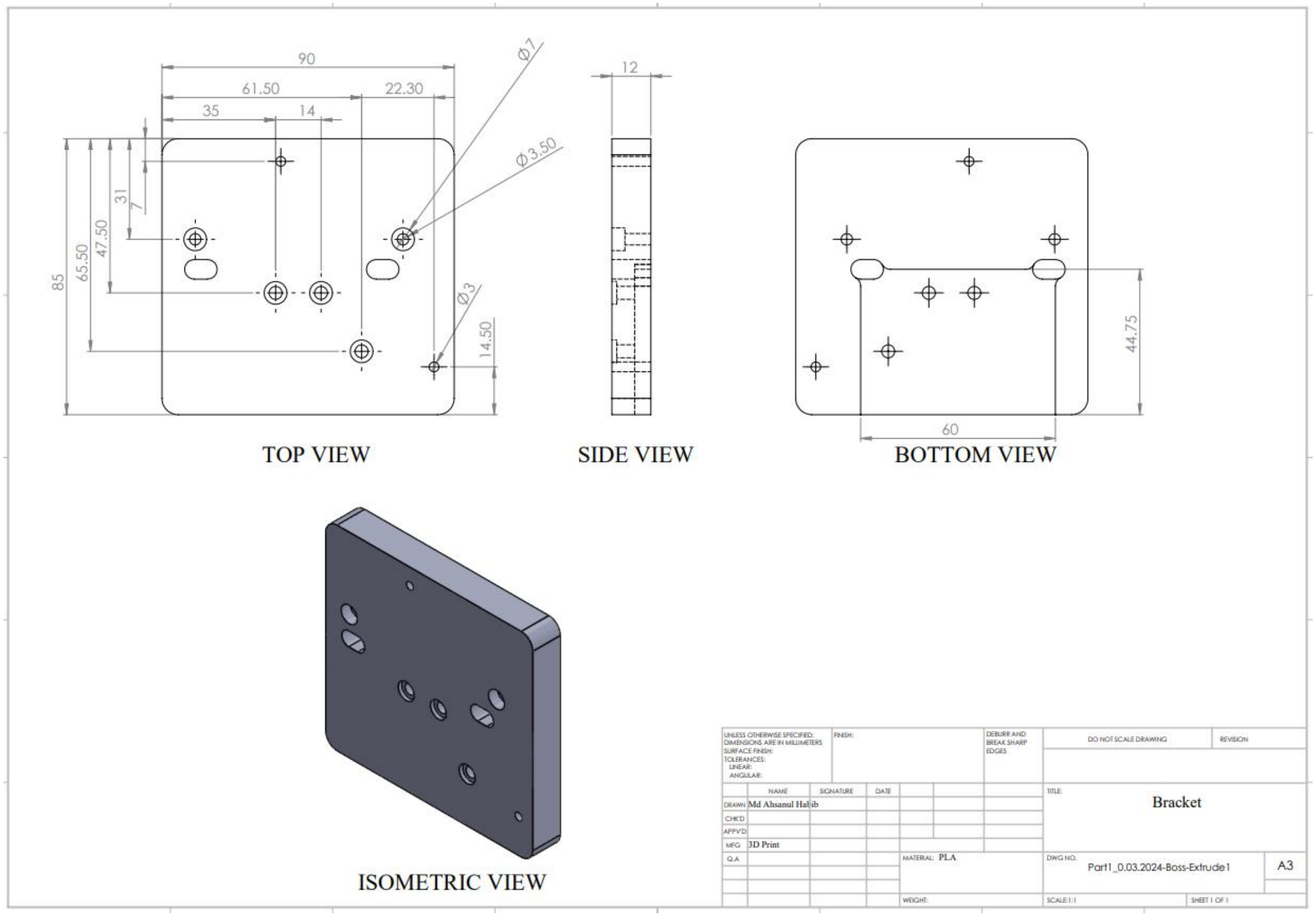

90
61.50
22.30
35
14
Ø7
Ø3.50
31
7
85
65.50
47.50
Ø3
14.50
12
44.75
60
TOP VIEW
SIDE VIEW
BOTTOM VIEW
ISOMETRIC VIEW
UNLESS OTHERWISE SPECIFIED:
DIMENSIONS ARE IN MILLIMETERS
SURFACE FINISH:
TOLERANCES:
LINEAR:
ANGULAR:
FINISH:
DEBURR AND BREAK SHARP EDGES
DO NOT SCALE DRAWING
REVISION
NAME
SIGNATURE
DATE
DRAWN Md Ahsanul Habib
CHK'D
APPV'D
MFG 3D Print
Q.A
MATERIAL: PLA
WEIGHT:
TITLE:
Bracket
DWG NO.
Part1_0.03.2024-Boss-Extrude1
A3
SCALE:1:1
SHEET 1 OF 1

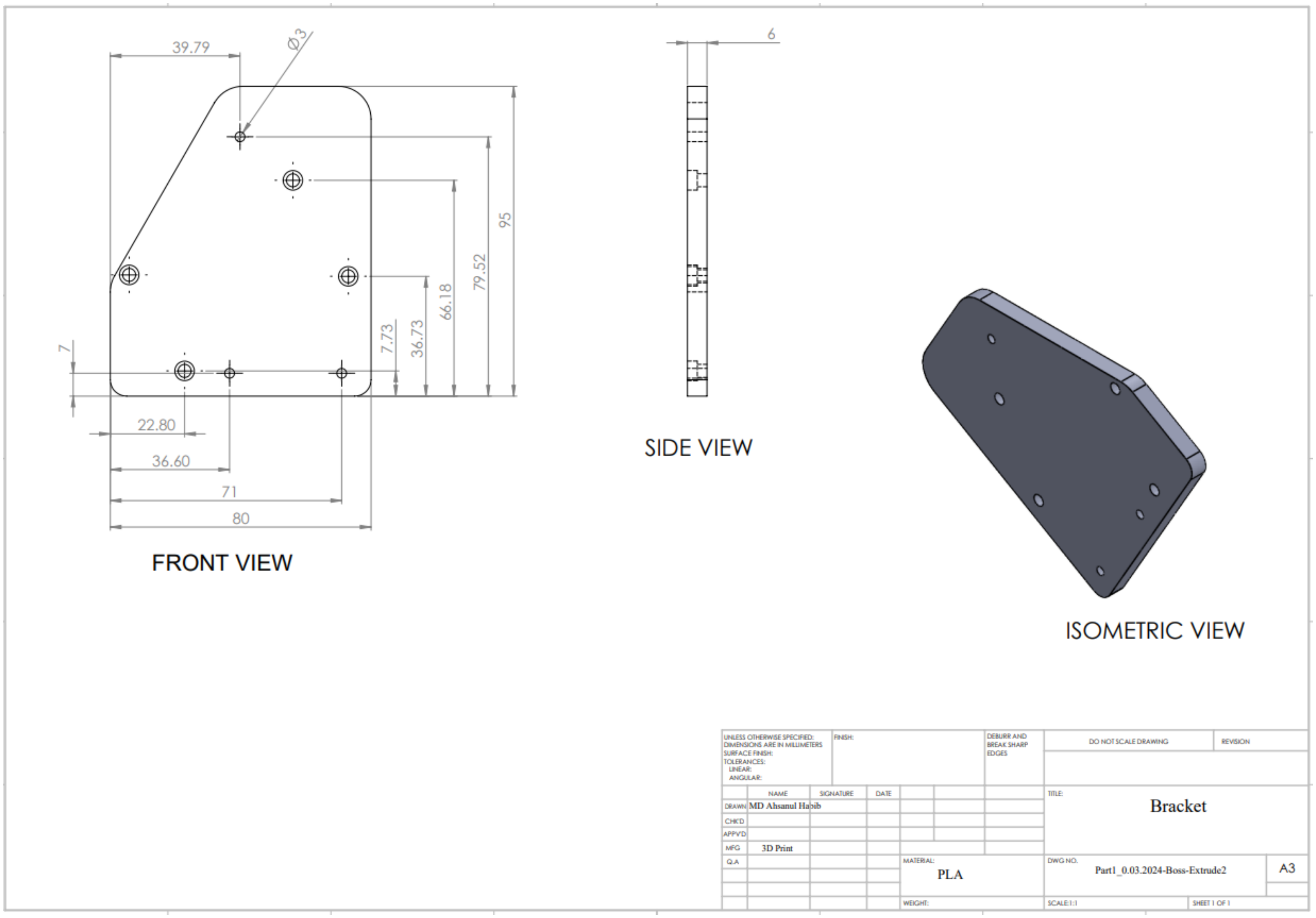
39.79
Ø3
6
95
79.52
66.18
36.73
7.73
7
22.80
36.60
71
80
FRONT VIEW
SIDE VIEW
ISOMETRIC VIEW
UNLESS OTHERWISE SPECIFIED:
DIMENSIONS ARE IN MILLIMETERS
SURFACE FINISH:
TOLERANCES:
LINEAR:
ANGULAR:
FINISH:
DEBURR AND BREAK SHARP EDGES
DO NOT SCALE DRAWING
REVISION
NAME
SIGNATURE
DATE
DRAWN
MD Ahsanul Habib
CHK'D
APPV'D
MFG
3D Print
Q.A
MATERIAL:
PLA
WEIGHT:
TITLE:
Bracket
DWG NO.
Part1_0.03.2024-Boss-Extrude2
A3
SCALE:1:1
SHEET 1 OF 1

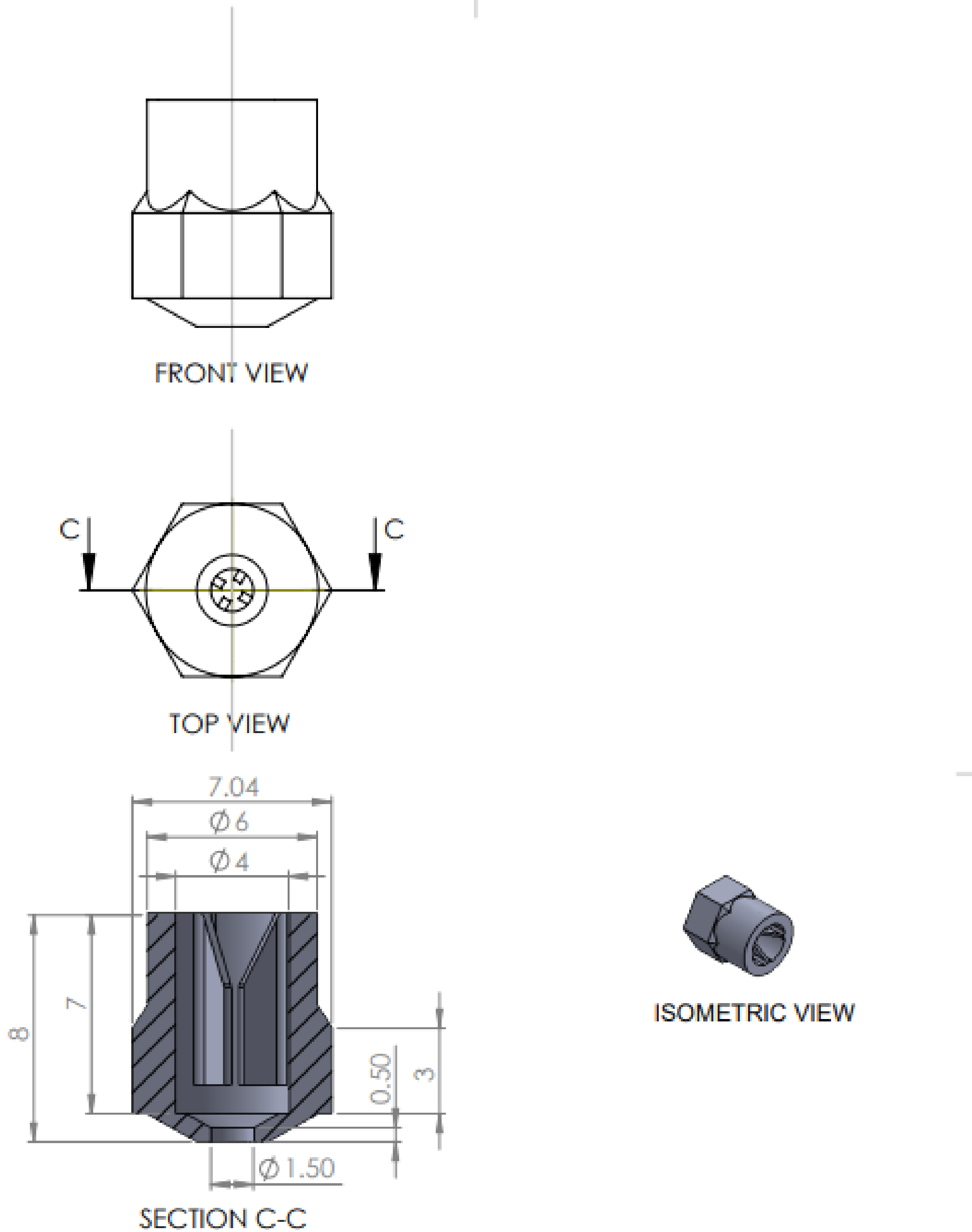

UNLESS OTHERWISE SPECIFIED:
DIMENSIONS ARE IN MILLIMETERS
SURFACE FINISH:
TOLERANCES:
LINEAR:
ANGULAR:

FINISH:

DEBURR AND BREAK SHARP EDGES

DO NOT SCALE DRAWING

REVISION

	NAME	SIGNATURE	DATE
DRAWN	MD Ahsanul Habib		
CHK'D			
APPV'D			
MFG	3D Print (SLM)		
Q.A			

TITLE: 1.5mm Nozzle

MATERIAL: Aluminum

DWG NO. Nozzle 1.5mm

A4

WEIGHT:

SCALE:5:1

SHEET 1 OF 1